The possible impact of Intermediate Mass Black Holes on our Galaxy

Wilhelm Krüger

Lund Observatory
Lund University

2014-EXA79

Degree project of 60 higher education credits (for a degree of Master)
May 2014

Supervisors: Melvyn B. Davies and Andreas Schrimpf

Lund Observatory
Box 43
SE-221 00 Lund
Sweden

Abstract

Orbit integration for three different assumed Intermediate-mass Black Hole (IMBH, defined as black holes with mass M_{BH} in the range $100M_{\odot} < M_{BH} < 10^4 M_{\odot}$) populations in the Milky Way for 10 Gyr has been performed. Upon collision with molecular clouds in the galactic disc, the relative velocity between both objects has been measured and the luminosity resulting from the gas accretion process onto the IMBH has been modeled. IMBHs moving on the very same orbits as today observed globular cluster do not create X-Ray luminosities during molecular cloud crossings exceeding $10^{39} \frac{erg}{s}$ with the exception of the disc-like orbit of NGC 6838. A population of $5.3 \cdot 10^5$ IMBHs, orbiting on similar orbits as globular cluster do, create on average 1 observable X-Ray object within the galactic disc at any given time. IMBHs orbiting within the galactic disc create high luminosities up to $10^{43} \frac{erg}{s}$ due to low relative velocities upon collisions. Assuming those disc-IMBHs have been created in cores of massive star cluster during the lifetime of the Milky Way, the fraction f of cluster creating IMBHs over all cluster capable of doing so has to be $f_A < 0.35$ ($f_B < 0.018$), otherwise ULXs (Ultraluminous X-Ray sources, luminosity $> 10^{39} \frac{erg}{s}$) are predicted to be visible at any given time, contradicting with observations. Index A refers to the model in which all cluster with masses $M_{cluster} > 5 \cdot 10^4 M_{\odot}$ can create IMBHs, while model B assumes cluster have only to obey $M_{cluster} > 2.5 \cdot 10^3 M_{\odot}$ to do so. In turn, given the different mass distributions within the IMBH population assuming model A or B, not more than about 15000 (A) or 16000 (B) IMBHs can be present today within the galactic disc. From the total number of IMBHs formed within star cluster in the disc, 49 % (A) or 54 % (B) have already lost their host cluster due to disruption in molecular cloud encounters. With the exception of NGC 6838, no globular cluster is expected to be destroyed via molecular cloud collisions within 10 Gyr.

Populärvetenskaplig sammanfattning

I detta projekt undersöks konsekvenserna av att anta förekomsten av Intermediate-mass black hole (IMBH, definerade som svarta hål med massa, M_{BH}, i intervallet $100M_\odot < M_{BH} < 10^4 M_\odot$) i vår galax. Medan stellar mass black holes ($M_{BH} < 100M_\odot$) är lätta att upptäcka i X-Ray-dubbelstjärnor, och supermassive-black holes ($M_{BH} > 10^4 M_\odot$) ligger i de flesta galaxers, centrum är förekomsten av IMBHs fortfarande omtvistad. Om ett IMBH kolliderar med ett gasmoln, fångar det upp en del av gasen vilket resulterar i observerbar röntgenstrålning. Antalet sådana händelser och den resulterande ljusstyrkan hos röntgenstrålningen undersöks för tre olika IMBH populationer. En sidofråga som måste besvaras är om, de ännu inte är helt klarlagda, extremt ljusa objekten i vissa andra galaxer, men inte vår kan förklaras med IMBHs som kolliderar med gasmolm eller inte. Den först undersökta IMBH-populationen gessamma banor som klotformiga stjärnhopar vilket är en rimlig uppsättning av galaktiska banor och som inte är, som för de flesta av stjärnorna i Vintergatan, begränsat till den galaktiska skivan och bara korsar den då och då. Detta gör det möjligt att undersöka effekterna av IMBHs på sådana icke-skivbanor. Men kollisioner med molekylmoln sker endast i den galaktiska skivan; sannolikheten att träffa ett moln i en passage genom skivan i de tätaste regionenerna är cirka 3%. Efter analysen av denna IMBH population kan slutsatsen dras, att den ljusstyrka som skapas i sådana kollisioner är i samma storleksordning som typiska röntgenbinärer innehållande ett stellar mass black hole, vilket gör det svårt att skilja mellan de båda fallen i observationer. För att förbättra statistiken och att övervinna den inneboende bristen av att endast ha ett begränsat antal banor, har en andra, slumpmässig population skapats. Banorna hos denna slumpmässiga population har liknande egenskaper som de klotformiga stjänhopparna, men varierar i hg grad när det gäller lutningen med avseende på skivan. Från resultaten av denna population kan slutsatsen dras att i genomsnitt $5,3 \cdot 10^5$ IMBHs som kretsar runt krävs för att skapa vid varje given tidpunkt, ett observerbart röntgen objekt. Den tredje IMBH populationen ligger i den Galaktiska skivan. Kollisionerna här är mycket mer frekventa och orsakar högre ljusstyrkor på grund av att den relativa hastigheten mellan de IMBHs och gasmolnen i allmänhet är låg; som den teoretiska härledningen visar är den relativa hastigheten den mest avgörande parametern vid bestämning av ljusstyrka. Som tidigare nämnts, är den ljusaste röntgenstrålningen inte observerbar i Vintergatan, men simuleringen bevis ar att IMBHs på skiv banor klarar av att skapa det. Detta begränsar därför antalet IMBHs som vistas i galaktiska skivan. Med detta argument kan vi dra, inte mer än 15000 eller 16000 IMBHs (beroende på den antagna massfördelningen för de IMBHs) kan kretsa Vintergatans skiva.

Acknowledgements

I would like to thank my supervisor Melvyn B. Davies for guiding me through my thesis and supporting me in any way possible. I would also like to thank my second supervisor Andreas Schrimpf for making it possible for me to write my thesis here in Lund and for giving helpful comments and insights.
I thank Anders Johansen and Bertram Bitsch for giving me valuable feedback on my draft thesis. Finally I like to thank the staff and students of the department for creating a friendly work atmosphere.
And of course I would like to thank Nina.

Contents

1 Introduction

This project investigates the expected impact of assumed Intermediate-mass Black Hole (IMBH, defined as black holes with mass M_{BH} in the range $100M_{\odot} < M_{BH} < 10^4 M_{\odot}$) populations orbiting in the Milky Way. The impact focused on, is the X-Ray luminosity resulting from gas accretion inside molecular clouds within the galactic disc. The methodology used consists of the numerical, computer based orbit integration of the IMBHs, modeling the molecular cloud population and gas accretion and measuring the relative velocity between IMBH and cloud upon collision. With these tools combined, the luminosity created in such collisions can be statistically investigated in terms of frequentness and dependency on orbital parameters of the IMBH such as the inclination with respect to the galactic disc or the eccentricity. Since the frequentness directly depends on the total number of IMBHs assumed, and given today's observed number of X-Ray sources, this in turn allows deriving an upper limit for the number of IMBHs present in the Milky Way today.
A side question to be answered is whether or not ULXs (Ultraluminous X-Ray sources, defined as off-nuclear objects with X-Ray luminosities exceeding $10^{39} \frac{erg}{s}$) can possibly be caused by IMBHs accreting in molecular clouds rather than by a (massive) binary system. Since no such ULX is observable in the Milky Way but in numerous nearby galaxies, this might be an important constrain for the possible number of IMBHs on orbits creating high luminosities.
The inherent problem with the project laid out so far are the unknown orbit properties of IMBHs in the Milky Way, assuming they exist at all. This defines the practical setup of the project, leading to the following three logically succeeding investigation steps:

1. In a first approach, globular cluster are used as an analog population, investigating the behaviour of IMBHs located outside the galactic disc and crossing it only occasionally. This is motivated on the theoretical side by suggested IMBH creation mechanisms found in literature which imply the existence of IMBHs in the halo rather than in the disc. On the observational side, some globular cluster are suspected to host IMBHs, making the analogy quite realistic. These information found in literature are explained and referenced in detail in section 2. The results are statistically analyzed focused on the expected luminosities upon molecular cloud collisions.

2. As a next step, a 'random' IMBH population is created and their impact investigated. The population is intended to represent an extension of the in number limited globuar cluster population from step 1. This is realized by creating orbits with eccentricities and mean distances from the galactic center which are similar to the globular cluster sample. Set random is the inclination of the orbits with respect to the galactic disc. This is motivated by the theoretical consideration, that the inclination is the orbital property most responsible for the luminosity created in collisions. Therefore, this population follows two general goals: The confirmation of results derived in step 1 by increasing the number of objects, and to find a direct relationship between orbital properties and resulting luminosity.

3. Interpreting the results from step 2, the most luminous IMBH orbits can be identified as orbits within the galactic disc. The investigation is focused on the possibility that IMBHs are created within massive star cluster. The implications of this scenario for IMBHs in terms of quantity, resulting luminosities and expected number of visible X-Ray sources today are analyzed in detail.

Concerning the models used, the orbit integration is carried out within a cylindric symmetric potential representing the gravity within the Milky Way. The molecular cloud distribution is modeled based on observed relations between cloud mass, radius and number. The number of clouds in turn depends on the distance from the galactic center, assuming again cylindrical symmetry. For simplicity and less computational expense, this is translated for the globular cluster analogy and the random population into a probability to hit a cloud upon entering the galactic disc from below/above. For the investigation of orbits within the disc, each molecular cloud is followed individually. The accretion rate inside the molecular clouds is modeled via the Bondi-Hoyle-accretion, resulting in a theoretical upper limit. Assuming a similar behaviour as in accretion discs formed in binary systems, the luminosity can be calculated. This derivation reveals a sensitive dependency of the luminosity on the relative velocity

between the IMBH and the molecular cloud.
In the course of the IMBH investigation in step 1 and 3, the impact of molecular clouds on globular cluster and cluster within the galactic disc is examined. First, this gives an answer towards the question, if it is surprising that globular cluster survived until today given the disruptive effect of multiple molecular cloud encounters, or not. Second, the probability that an IMBH formed in a cluster lost its host can be derived.

This report is organized as follows:
Section 2 summarizes the background and already done research found in the literature related to this project, section 3 derives the basic equations and models used, namely the orbit integration and accretion, section 4 concerns the globular cluster analogy including the simplified molecular cloud model, section 5 improves the globular cluster statistic with the help of a random population, section 6 examines the impact of IMBHs orbiting within the disc and motivates their existence and section 7 is dedicated to the globular cluster destruction via molecular clouds. Section 8 summarizes the results.

2 Background

This section summarizes previous work found in the literature related to my project and gives a broader background. This gives an overview about how my project fits into current research.

2.1 Orbit integration

In order to integrate orbits of objects of any kind in the Milky Way, the gravitational potential of the galaxy in an analytical closed form is needed. Different expressions with parameters found by fitting to observations have been proposed in the literature. Paczynski (1990) used a superposition of three potentials describing the influence of different parts within the galaxy: axissymmetric Miyamoto-Nagai (Miyamoto & Nagai, 1975) potentials for the galactic disc and the galactic bulge, and a spherical symmetric potential for the dark matter halo. Allen & Santillan (1991) introduced a similar three component potential. It consists in the same way of Miyamoto-Nagai disc potential, but uses a spherical symmetric bulge and a different expression for the halo. One method to verify the accuracy of different galactic potentials is to calculate the velocity which an object orbiting within the plane of the galactic disc needs in order to be circular (i.e. the distance R from the galactic center is constant). This velocity v_c depends on R and is therefore plotted in an v_c - R diagram called the rotation curve. The capability of the rotation curve to reproduce the observed mean motion of stars for different R is used to evaluate the quality of the model. Despite the differences of the above models, both rotation curves are able to fit the observations equally well due to high uncertainties in the observed values especially in the dark matter halo. Irrgang et al. (2013) improved the potential proposed by Allen & Santillan (1991) by using new observational constraints and modifying the expression for the dark matter potential. However, the differences of the resulting rotation curve towards the rotation curve of Paczynski (1990) are smaller than the errorbars of the new observational constrains, especially for the dark matter halo. The same argument holds for a different potential presented by Law & Majewski (2010) which main difference is the use of a non-sperical halo potential. Given this equality in capability of reproducing the observations and the slightly simpler expression for the dark matter halo, the Paczynski (1990) model is used in this work. For simplicity, non-axissymmetric potentials describing the bar structure in the bulge (Pichardo et al., 2004) or the spiral arm structure of the disc ((Binney & Tremaine, 1987); (Pichardo et al., 2003)) are not considered.
Orbit integration especially for globular clusters has been done by Odenkirchen et al. (1997) using the Allen & Santillan (1991) potential, Casetti-Dinescu et al. (2013) using a by Carlin et al. (2012) improved Law & Majewski (2010) potential, Allen et al. (2008) using the Allen & Santillan (1991) potential and comparing it to non-axissymmetric potentials, Shu et al. (2010) using the Paczynski (1990) potential, and Irrgang et al. (2013) using the described improved Allen & Santillan (1991) potential.
A compilation of the known position and proper motions of 63 globular cluster needed as inital conditions for orbit integration can be found online [1]. The positions are obtained from the Harris catalogue (Harris, 1996), the proper motions have been collected from Cudworth et al. (1993), Odenkirchen et al. (1997), Dinescu et al. (1997), Dinescu et al. (1999a), Dinescu et al. (1999b), Dinescu et al. (2003), Casetti-Dinescu et al. (2007), Casetti-Dinescu et al. (2010) and Casetti-Dinescu et al. (2013).

2.2 Molecular clouds

The interstellar medium within the Milky Way mostly contains molecular H_2 gas which clusters together into molecular clouds ((Solomon & Sanders, 1980); (Scoville & Sanders, 1987)) with cloud masses between 10^4 and $10^7 M_\odot$ (Hou et al., 2009). About 90% of the total H_2 mass is contained within self-gravitating giant molecular clouds (Mass $M > 10^5 M_\odot$) ((Scoville & Sanders, 1987); (Solomon et al., 1987)). Since H_2 is a light molecule with no permanent dipole moment, it has no permitted emissions in radio frequencies and is therefore difficult to detect; instead, a by H_2 collisions induced CO transition

[1] http://www.astro.yale.edu/dana/gc.html

is used as an H_2 tracer (Scoville & Sanders, 1987). The cloud mass is then derived from the observed cloud size and its internal velocity dispersion assuming virial equilibrium. Statistically, the number of found clouds with given properties (mass, size, dispersion) scales with the property values in simple power laws ((Larson, 1981); (Heyer et al., 2009); (Scoville & Sanders, 1987)). In terms of spatial distribution, molecular clouds are confined within the galactic disc with a scale height of about $75pc$ (Krolik, 2004). They can be used as tracer for spiral arms (Hou et al., 2009). This manifests in the first galactic quadrant into an increased cloud concentration for distances from the galactic center between about 4 and 6 kpc (Clemens et al., 1988); extrapolated towards the full disc, this is called in this work the molecular ring.

2.3 Accretion

Accretion in this work is defined as the process of accumulating mass onto a gravitating object. The Bondi-Hoyle accretion is an analytical model proposed by Bondi & Hoyle (1944) and Hoyle & Lyttleton (1939) for describing the time dependent matter flow onto a gravitating point mass which moves through a gas cloud (Edgar, 2004). Due to the movement, material accumulates in a wake behind the point mass and gets slowly accreted due to friction within the wake. Although this formalism provides useful approximations for most applications, it does not cover more realistic, less idealized situations. Most notable, if the gas has a net angular momentum, an accretion disc is formed, thus destroying symmetry and introducing different new physical effects (e.g. Park & Ricotti (2011)). In this disc case, the lost gravitational potential energy heats up the disc via friction, creating black body radiation peaking typically in X-Ray (see McClintock (2004) for a review). Another effect is radiative feedback: the momentum of the emitted non-escaping photons act against the gravitational pull towards the gas and therefore reduces the accretion rate, which in turn leads to an decrease of the temperature and therefore to less energetic photons. If the gravitational pull and the photon momentum are balanced, the corresponding luminosity resulting from the escaping photons is called the Eddington luminosity; this therefore defines the theoretical highest possible luminosity emitted by an accreting object (Rybicki & Lightman, 1979). See section 3.2 for a detailed derivation. Note here, that the Eddington luminosity is proportional to the mass of the gravitating object. Additionally, as shown in hydrodynamical simulations done by Park & Ricotti (2011), radiative feedback induces oscillations in the accretion, causing that only in about 6% of the accretion time the peak luminosity is actually reached.

2.4 Stellar mass black holes

Stellar mass black holes are supernova explosion remnants of massive stars and do not exceed $80M_\odot$ (Kocsis & Loeb, 2013). They are easiest detectable in stellar binaries due to the X-Ray luminosity created by the accretion of mass from the companion star (Casares & Jonker, 2013). Those black hole X-Ray binaries can be divided into two subgroups: Low-mass X-Ray binaries (LMXBs) and high-mass X-Ray binaries (HMXBs), depending on the mass of the companion star (Kocsis & Loeb, 2013). In low-mass X-ray binaries (LMXBs), the low-mass companion star fills and overflows its Roche lobe, enabling the black hole to accrete the excessive mass. In high-mass X-ray binaries (HMXBs), the high-mass companion ejects a dense wind which the black holes accrete; Roche lobe overflow is possible but rare (Chaty, 2013). A catalogue containing 187 LMXBs has been published by Liu et al. (2007), a catalogue containing 114 HMXBs by Liu et al. (2006). Of this, 113 LMXBs and 64 HMXBs have no orbital period listed, leaving room for the speculation in this project, that those objects might in fact not be binaries. The X-Ray luminosity of the objects with known distance from the sun ranges from $10^{33}\frac{erg}{s}$ to several $10^{38}\frac{erg}{s}$. A lower limit for the mass of the black hole is most robustly calculated by radial velocity measurements of the companion star. An estimation for the exact mass with this technique however requires knowledge about the difficult to obtain inclination of the binary ((Casares & Jonker, 2013); (Zhang, 2012)). For LMXBs, the black hole mass distribution has been modeled as a Gaussian with mean at $7.8M_\odot$ and $1-\sigma$ spread of $1.2M_\odot$ by Özel et al. (2010). Prestwich et al. (2007) found in the HMXB system IC 10 X-1 an exceptional high massive stellar black hole of $\approx 24-34M_\odot$.

2.5 Supermassive black holes

Supermassive black holes ($10^6 - 10^{10} M_\odot$) are observed in the center of most galaxies (Casares & Jonker, 2013). The mass can be derived by observing the motion of stars and gas orbiting the central object (e.g. Ghez et al. (2008)). If the black hole is associated with an active galactic nucleus, defined as a region of increased luminosity within the galaxy, then another possibility is applying reverberation mapping towards the emission lines, which uses the doppler effect of photons escaping the accretion disc in order to determine the keplerian speed of the disc and hence the mass of the central object (Peterson, 2013). The formation process of Supermassive black holes especially in the early universe is subject to current research. Black holes with masses of $\approx (1-2) \cdot 10^9 M_\odot$ have been detected at redshift $z > 6.5$, corresponding to an age of the universe of less than 1Gyr ($\approx 7 \cdot 10^8$ years) (Venemans et al., 2013). This leads to the problem, that since even the first generation of stars (so called Population III stars) need a few 10^8 years to form (Inoue et al., 2014) and, if massive enough, collapse into a stellar mass black hole seed of $100 M_\odot$, accretion at the Eddington limit resulting in an exponential growth with the salpeter timescale $5 \cdot 10^7 yr$ needs about $5 \cdot 10^7 \cdot \ln\left(\frac{10^9}{100}\right) = 8 \cdot 10^8$ years to grow a supermassive black hole of mass $10^9 M_\odot$ ((Haiman, 2013) ; (Volonteri, 2010); (Kocsis & Loeb, 2013)). Additional to that these timescales barely fit to explain fast enough growth to explain early supermassive black holes, permanent Eddington accretion is an unlikely assumption ((Madau et al., 2014); (Kocsis & Loeb, 2013); (Park & Ricotti, 2011)). Other mechanisms to overcome these assumptions have been proposed, including direct gas collapse into bigger seeds, merging of black holes or super-Eddington accretion. See Haiman (2013) for a review.

2.6 Intermediate-mass black holes

This just described and not yet fully understood formation process of supermassive black holes naturally involve Intermediate-mass Black Holes ($100 - 10^4 M_\odot$) as an intermediate step. This leads to the question of direct observational evidence for IMBHs not only to confirm or discard the evolution process of SMBHs, but also as a study field on its own. So far, the existence of IMBHs is still in dispute ((Rashkov & Madau, 2014) ; (Webb et al., 2012); (Casares & Jonker, 2013)), but evidence hardens. Valencia-S et al. (2012) and (Dewangan et al., 2008) report the detection of IMBHs in galactic centers. For off-nuclear IMBHs, defined as IMBHs not located in the galactic center, globular cluster are possible candidates: Kinematics of stars in globular cluster suggest IMBHs reside in their center ((Lützgendorf et al., 2013); (Feldmeier et al., 2013); (Umbreit & Rasio, 2013); (Noyola et al., 2008)). The expected X-Ray luminosity of a globular cluster accreting IMBH is low due to the lack of gas (Sun et al., 2013). However, the fundamental plane relation ((Maccarone, 2004); (Plotkin et al., 2012)) links the easier observable radio luminosity with the black hole mass, suggesting again the existence of IMBHs in certain globular cluster ((Sun et al., 2013); (Nyland et al., 2012)). On the theoretical side, the creation of IMBHs in globular cluster seems possible via stellar collisions ((Portegies Zwart & McMillan, 2002); (Goswami et al., 2012); (Freitag et al., 2006)) or a combination of accretion and black hole mergers (Miller & Hamilton, 2002).
Besides the mentioned formation in clusters, IMBHs may in general form out of two mechanisms: The growth of massive PopIII black hole remnant in the pregalactic halo via accretion and/or merging ((Tanaka & Haiman, 2009); (Volonteri et al., 2003)) or the direct gravitational collapse of gas (Mayer et al., 2010). Rashkov & Madau (2014) statistically investigated the consequences of both mechanisms and concludes the presence of several hundred up to few thousand remnant IMBHs present in the Milky Way halo today. Kuranov et al. (2007) investigated the creation of IMBH binaries originated from the Pop-III mechanism, and concluded, that too many ULX (see below) are observed today to be explained by accreting IMBH binaries. However, IMBH binaries may also form within young dense star cluster within the galactic disc (Portegies Zwart, 2010).

2.7 Ultra luminous X-Ray sources

Another piece of evidence for off-nuclear IMBHs has been found in Ultra-luminous-X-Ray sources (ULXs), defined as off-nuclear point sources with X-Ray luminosity exceeding $10^{39} \frac{erg}{s}$, observed in nearby galaxies but not in the Milky Way (e.g. Caballero-García et al. (2013)). Although there are more than 400 ULXs known, their nature remains unclear (Pintore et al., 2014). The spectra of some of these objects resembles those of stellar mass black hole binaries but exceed their Eddington luminosity. This leads to the possible explanation of a more massive IMBH accreting rather than a stellar mass black hole ((Makishima et al., 2000) ; (Miller, 2006); (Makishima, 2007); (Fabbiano, 2006)). However, also other explanations without involving an IMBH, such as beaming (King et al., 2001) or super-Eddington emission (Begelman, 2002), have been proposed. ULXs are mostly associated with star forming regions (e.g. Mezcua et al. (2014)), leading to contaminations in the spectra and making mass estimations via radial velocity measurements difficult (González-Galán et al., 2013).
Another possible explanation for ULX are IMBHs accreting within molecular clouds (Krolik, 2004), which is explained in detail in this thesis.

3 Modeling

3.1 Orbit integration

The first step in investigating the interactions between objects in the Milky Way, such as the collisions between IMBHs and molecular clouds, is to calculate the trajectory of their orbits. This is done by numerically integrating the initial conditions (3-Dimensional position x_0, y_0, z_0 and velocity $v_{x,0}, v_{y,0}, v_{z,0}$) of each object under the influence of the gravitational potential of the Milky Way.
Throughout this thesis, the galactic cartesian coordinate system is defined as follows: x points from the galactic center into the direction of the sun, y into the direction of the rotation of the galactic disc, and z towards the galactic north pole (which is uniquely defined by demanding a right-handed coordinate system).
As described in section 2, the Milky Way potential used follows Paczynski (1990). In detail, the model consists of a superposition of two cylindric symmetric Miyamoto-Nagai potentials (Miyamoto & Nagai, 1975) ψ_d and ψ_b for representing the galactic disc and the bulge, respectively, and a spherically symmetric potential ψ_h for the dark matter halo:

$$\psi_d(R,z) = -\frac{GM_d}{\sqrt{R^2 + \left(a_d + \sqrt{z^2 + b_d^2}\right)}} \qquad \psi_b(R,z) = -\frac{GM_b}{\sqrt{R^2 + \left(a_b + \sqrt{z^2 + b_b^2}\right)}} \tag{1}$$

$$\psi_h(r) = \frac{GM_c}{r_c}\left[\frac{1}{2}\ln\left(1 + \frac{r^2}{r_c^2}\right) + \frac{r_c}{r}\arctan\left(\frac{r}{r_c}\right)\right] \tag{2}$$

with $R = \sqrt{x^2 + y^2}$, $r = \sqrt{x^2 + y^2 + z^2}$, G the gravitational constant. The parameters are:

$$\begin{array}{llll} a_d = 0 & pc & b_d = 277 & pc \\ a_b = 3700 & pc & b_b = 200 & pc \\ & & r_c = 6000 & pc \end{array} \qquad \begin{array}{ll} M_d = 1.12 \cdot 10^{10} & M_\odot \\ M_b = 8.07 \cdot 10^{10} & M_\odot \\ M_c = 5 \cdot 10^{10} & M_\odot \end{array} \tag{3}$$

The total Milky Way potential ψ is then defined as $\psi = \psi_d + \psi_b + \psi_h$. Note here, that the zero point of the three potential contributions is not at the same level. For the disc and bulge it is set to infinity:

$$\lim_{R\to\infty} \psi_{d/b}(R,z) = \lim_{z\to\infty} \psi_{d/b}(R,z) = 0 \tag{4}$$

Whereas for the dark matter halo:

$$\lim_{r\to\infty} \psi_h(r) = \infty, \quad \lim_{r\to 0} \psi_h(r) = \frac{GM_c}{r_c} \tag{5}$$

However, since only the derivative of the potential $\nabla\psi = \nabla\psi_d + \nabla\psi_b + \nabla\psi_h$ is the essential quantity as explained below, different zero points between the contributing potentials only add in the derivation negligible constants.
The corresponding density distributions ρ can be calculated by solving the poisson equation $\rho = \nabla^2\psi$ (Miyamoto & Nagai, 1975):

$$\rho_{d,b}(R,z) = b^2 M \frac{aR^2 + \left[a + 3\sqrt{z^2 + b^2}\right] \cdot \left[a + \sqrt{z^2 + b^2}\right]^2}{4\pi\left[R^2 + (a + \sqrt{z^2 + b^2})^2\right]^{5/2} \cdot (z^2 + b^2)^{3/2}} \tag{6}$$

$$\rho_h(r) = \frac{M_c}{4\pi r_c^3 \cdot \left(1 + (r/r_c)^2\right)} \tag{7}$$

For each time step Δt, the acceleration of each object due to the force of the gravitational potential ψ is calculated according to Newton's law

$$\frac{d^2\vec{r}}{dt^2} = -\nabla\psi \tag{8}$$

For N objects this delivers 3N second order differential equations, which can be rewritten into 6N first order equations:

$$\frac{d\vec{r}}{dt} = \vec{v} \tag{9}$$

$$\frac{d\vec{v}}{dt} = -\nabla\psi \tag{10}$$

The derivative $\nabla\psi$ can be analytically calculated. The trajectory for all N objects are found by numerically integrating (9) and (10) starting with 6N initial conditions.
For trivial cases, the trajectory can be found directly analytically and gives insight in the properties of the used galactic model. For z = 0, for each distance $R = \sqrt{x^2 + y^2}$ a circular orbit can be found which has a constant rotation velocity v_c. This velocity can be calculated by balancing gravity with the centrifugal force:

$$\begin{aligned} |\nabla\psi| &= \frac{v_c^2}{R} \\ \Rightarrow v_c &= \sqrt{R \cdot |\nabla\psi|} \end{aligned} \tag{11}$$

As pointed out in section 2.1, a plot of v_c versus R is called the rotation curve and is for the here used potential presented in figure 1.
For huge distances, the rotation velocity becomes a constant:

$$v_c = \sqrt{G\left(M_s \frac{R^2}{\left(R^2 + (a_s + b_s)^2\right)^{3/2}} + M_d \frac{R^2}{\left(R^2 + (a_d + b_d)^2\right)^{3/2}} + \frac{M_h}{r_c}\left[1 - \frac{r_c}{R}\arctan\left(\frac{R}{r_c}\right)\right]\right)}$$

$$\rightarrow \lim_{R\to\infty} v_c = \sqrt{G\frac{M_h}{r_c}} = 189\frac{km}{s} \tag{12}$$

Another useful aspect of the potential is the property, that all objects are necessarily bound to the Milky Way independent of their speed. In order to proof this, the escape velocity $v_{esc,h}$ of the in huge distances dominating halo potential can be calculated by balancing the kinetic energy with the potential energy:

$$\begin{aligned} \frac{1}{2}v_{esc,h}^2 &= |\psi_h| \\ \Rightarrow v_{esc,h} &= \sqrt{2|\psi_h|} \end{aligned} \tag{13}$$

This relationship is plotted in figure 1. For huge distances,

$$\lim_{r\to\infty} v_{esc,h} = \sqrt{2\frac{GM_c}{r_c}\left[\frac{1}{2}\ln\left(1 + \frac{r^2}{r_c^2}\right) + \frac{r_c}{r}\arctan\left(\frac{r}{r_c}\right)\right]}$$

So due to the logarithm,

$$\lim_{R\to\infty} v_{esc,h} = \infty \tag{14}$$

Meaning the energy necessary to increase the distance from the galactic center to infinity is also infinity, making an escape impossible. The reason for this behaviour is the density distribution ρ_h which leads to an infinite amount of mass M_{halo} in the halo and therefore in the whole galaxy:

$$\begin{aligned} M_{halo}(r) &= 4\pi \int_0^r \rho_{halo}(r')\ r'^2 dr' \\ &= \frac{M_c}{r_c^3} \int_0^r \frac{1}{1+\left(\frac{r'}{r_c}\right)^2}\ r'^2 dr' \\ &= \frac{M_c}{r_c}\left(r - r_c \arctan\left(\frac{r}{r_c}\right)\right) \end{aligned} \tag{15}$$

Therefore,

$$\lim_{r\to\infty} M_{halo}(r) \propto r \tag{16}$$

Meaning the model assumes a linear increase of the total mass with r for huge distances. This increase in mass then in turn leads to an increase of the potential energy as shown in equation (14). Note here, that the common simplification of ψ for huge distances r into a spherical potential with all total mass $M \propto r$ concentrated in the center, which would result into

$$\psi = \frac{G\ M}{r} = \frac{G\ r}{r} = const, \tag{17}$$

does not hold. The reason for this is, that since the mass spreads towards infinity, an object can never be at a distance where a further increase of the distance does not add new mass. If for clarity this problem would be transfered onto the gravitational potential of the earth, the infinite increasing mass would mean, that an object can never reach earths surface at which (17) would be valid.
As mentioned, this behaviour of the potential to keep all objects bound is desirable, since the simulations investigate the impacts of objects crossing the disc. Objects escaping the Milky Way do not contribute to the statistic and need unnecessary computational time.

The orbit integration is done numerically on a computer using a combination of python and C++ as programming languages. As a reasonable compromise between speed and accuracy, (9) and (10) are solved by a 4th-order Runge-Kutta integrator. Since the total energy of an object orbiting in the presented Milky Way potential is a conserved quantity, the energy conservation is used as a measurement of the error done in the integration and in turns constrains the allowed step size: If E_0 is the total kinetic and potential energy of an object at time t, and E the total energy after one time step $t + \Delta t$ has been performed by the integrator, then an adaptive step size routine decreases Δt until at least $\frac{|E-E_0|}{|E_0|} < 1 \cdot 10^{-6}$ for each integrated object is fulfilled.

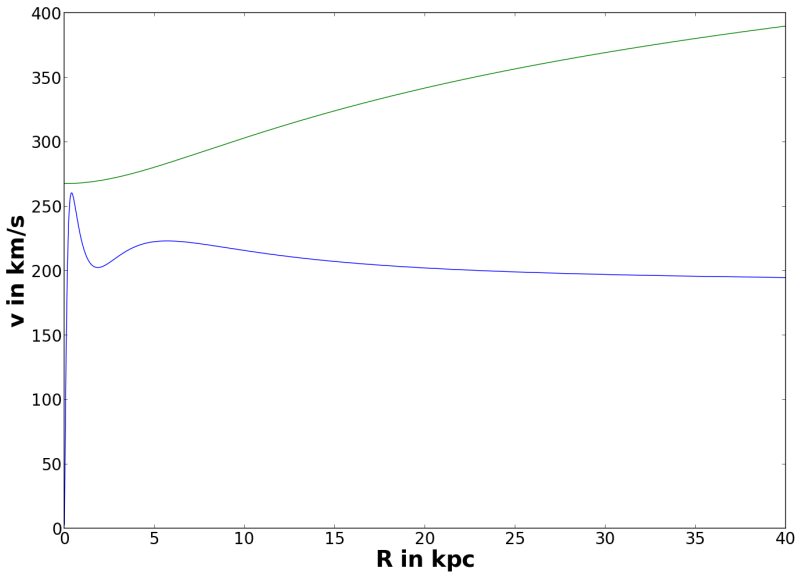

Figure 1: *Blue: rotation velocity v_c of the Milky Way potential. Green: escape velocity $v_{esc,h}$ for the halo potential. Both curves assume $z = 0$.*

3.2 Accretion

In this section, an upper limit for the accretion rate and resulting X-Ray luminosity of a black hole entering a molecular cloud is derived.
The black hole is modeled as a point object with mass M_{BH} which moves with the relative velocity v_{rel} through the molecular cloud. The molecular cloud is assumed to be a field of homogenous gas of constant density ρ. The thermal motion within the few Kelvin cold cloud is neglected compared to typically v_{rel} in the order of tens to a few hundred km/s (compare figure 9).
For the case of a black hole, the Bondi-Hoyle radius r_b is defined as the distance from the black hole at which the kinetic energy of the gas particle is equal to the gravitational potential energy due to the black hole. All particles within this radius are slower than the escape speed and therefore gravitationally bound. r_b is given by:

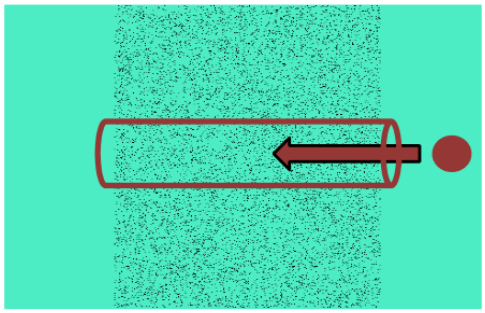

Figure 2: *Scheme for the Bondi-Hoyle accretion: The IMBH enters a field of constant density and accretes all particles within r_{Bond}.*

$$\begin{aligned} |E_{kin}| &= |E_{pot}| \\ \rightarrow \frac{1}{2} v_{rel}^2 &= \frac{GM_{BH}}{r_b} \\ \rightarrow r_b &= 2\frac{GM_{BH}}{v_{rel}^2} \end{aligned} \tag{18}$$

As an upper limit, it is assumed that all particles which become gravitationally bound during the motion of the black hole through the molecular cloud are being instantaneously accreted.
In reality, the bound particles are first focused in a wake following the black hole motion. Friction within

the wake then enables particles to collide with the black hole, resulting in a delayed accretion which finishes after the black hole has already left the cloud. See Edgar (2004) for a review covering this more complex model.
As sketched in figure 2, all accreted particles are located within a cylinder of radius r_b and length

$$2R_{cloud} = v_{rel}\Delta t \tag{19}$$

with R_{cloud} the radius of the molecular cloud and Δt the time spent within the cloud. The total accreted mass ΔM is therefore given by

$$\Delta M = \pi r_b^2 \rho \cdot v_{rel}\Delta t \tag{20}$$

Using (18) and the assumption that all particles are instantaniously accreted,

$$\dot{M} = \frac{\Delta M}{\Delta t} = 4\pi \frac{G^2 M_{BH}^2}{v_{rel}^3}\rho \tag{21}$$

which represents an upper limit for the accretion rate.
In order to put radii into context, for a massive black hole with $M_{BH} = 10^4 M_\odot$, $r_b = 0.009pc$. This is small compared to the radii of molecular clouds which is of the order of a few up to tens of pc (compare to equation (49)). The schwarzschild radius r_s of a black hole,

$$r_s = \frac{2GM_{BH}}{c^2} \tag{22}$$

results for $M_{BH} = 10^4 M_\odot$ in $r_s = 3 \cdot 10^{-4}\ pc$.

Although the formation of a wake is neglected, its presence is essential for converting kinetic energy into photons which create a black body spectrum with a peak in the X-Ray regime and luminosity L. The energy lost due to the photons equals a mass loss $\dot{m}$ according to the time derivative of the mass-energy relation,

$$E = mc^2 \tag{23}$$

$$\rightarrow L = \dot{m}c^2 \tag{24}$$

with c the speed of light. Assuming an accretion rate $\dot{M}$, a fraction of the matter is converted to energy according to equation (24), the rest falls into the black hole. The efficiency of this conversion is called μ and is for a thin stellar mass black hole accretion disc of the order $\mu \approx 0.1$ (Park & Ricotti, 2011), which is also used here:

$$L = \mu \dot{M} c^2 \tag{25}$$

Using equation (21) and the mass - radius relation for molecular clouds from equation (49) for $\beta = 0.55$ and $k = 0.5$,

$$\begin{aligned} L &= 4\pi\mu \frac{G^2 M_{BH}^2}{v_{rel}^3}\rho c^2 \\ &= 5.2\ \mu \cdot 10^{40} \left(\frac{M_{BH}}{M_\odot}\right)^2 \left(\frac{km/s}{v_{rel}}\right)^3 \left(\frac{M_{cloud}}{M_\odot}\right)^{-0.43} \frac{erg}{s} \end{aligned} \tag{26}$$

Figure 3 is a plot of (26) for lines of constant luminosity assuming a cloud mass of $M_{cloud} = 10^7 M_\odot$. The plot emphasizes the sensitive dependence of the luminosity on the black hole mass and the relative velocity. For a massive IMBH of $M_{BH} = 10^4 M_\odot$, a luminosity of $L > 10^{39} \frac{erg}{s}$, the luminosity of ULXs (section 2.7), requires relative velocities of below $100 \frac{km}{s}$. A luminosity of $L = 10^{41} \frac{erg}{s}$ requires about $20 \frac{km}{s}$.

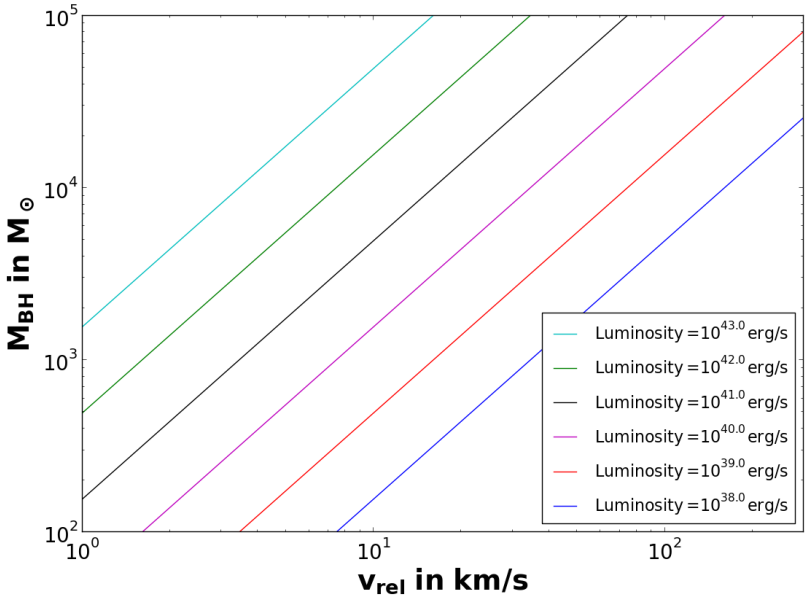

Figure 3: *Lines of constant luminosity due to accretion of an IMBH within a molecular cloud of* $10^7 M_\odot$ *for different IMBH masses* M_{BH} *and relative velocities* v_{rel}.

Another important physical aspect concerning high luminosities is radiative feedback. Ignoring once again the motion of the black hole with the forming wake and using the picture of a homogeneous spherical shell of gas around the black hole, then the gas heats up due to friction which allows particles to spiral into the black hole. The heated gas emits photons, observable as the black body radiation. Photons which are reabsorbed by incoming particles accelerate them outwards, effectively decreasing the accretion rate $\dot{M}$. This in turns reduces the friction and temperature in the shell, reducing the photon pressure. The equilibrium between both processes is called the Eddington Limit and represents a theoretical upper limit for the accretion rate and therefore luminosity.
The photon flux f is the emitted energy dE per area dA per time dt,

$$f = \frac{dE}{dA\ dt} \tag{27}$$

Only a fraction of the emitted photons is reabsorbed by incoming atoms. To give a lower limit on radiative feedback, pure Thomson-scattering of completely ionized hydrogen with cross-section σ_T is assumed. The energy E of the photons correlates with their impuls p as $E = pc$, so

$$f = \frac{c\ dp}{\sigma_T\ dt} = \frac{c}{\sigma_T} F_{photon} \tag{28}$$

with F_{photon} the force on a single electron inflicted by photons. Since the total flux is isotropicall over the whole area of the shell at distance r from the black hole, the luminosity L is given as:

$$L = 4\pi r^2 f \tag{29}$$

Assuming the impuls is carried via electromagnetism from the electron towards the whole hydrogen atom with mass m_H, the resulting force per mass is given by

$$\frac{F_{photon}}{m_H} = \frac{\sigma_T}{m_H} \frac{L}{4\pi r^2 c} \tag{30}$$

If the force is equal to the gravitational force per mass F_{grav},

$$\frac{F_{grav}}{m_H} = -\frac{GM_{BH}}{r^2} \tag{31}$$

then the Eddington luminosity L_{Edd} is reached:

$$\frac{\sigma_T}{m_H}\frac{L_{Edd}}{4\pi r^2 c} = \frac{GM_{BH}}{r^2}$$

$$\rightarrow L_{Edd} = 4\pi c G M_{BH}\frac{m_H}{\sigma_T} \tag{32}$$

For $\sigma_T = 6.65 \cdot 10^{-25} cm^2$ (Rybicki & Lightman, 1979),

$$L_{Edd} = 1.26 \cdot 10^{31}\left(\frac{M_{BH}}{M_\odot}\right)\frac{kg\ m^2}{s^3} = 1.26 \cdot 10^{38}\left(\frac{M_{BH}}{M_\odot}\right)\frac{erg}{s} \tag{33}$$

which is an upper limit for the accretion luminosity. This directly visualizes, that stellar mass black holes with $1M_\odot < M_{BH} < 10M_\odot$ can not cause luminosities of $L > 10^{39}\frac{erg}{s}$. The easiest solution if such a luminosity is observed is the assumption of an IMBH accreting ($100M_\odot < M_{BH} < 10^4 M_\odot$).

4 Globular cluster population

4.1 Overview

The first method used in this project focuses on the possibility that IMBHs are located in the halo of the Milky Way rather than within the galactic disc. This is motivated by in section 2.6 presented different creation mechanisms such as growth via accretion starting with early PopIII stars, direct gravitational gas collapse or merging mechanisms in star cluster. Additionally observation of kinematics in certain globular cluster suggest the presence of IMBHs in their cores. In contrast to stellar mass black holes which are an end product of stellar evolution and therefore frequently located in bright binaries, IMBHs are expected to be mostly single, dark objects. The simulation carried out in this section answers the question, if IMBHs can be detectable while passing molecular clouds.
Due to the difficult detection of IMBHs, their general spatial distribution and number in the Milky Way is unknown. As an first approximation, the orbits of globular cluster as galactic objects located mostly in the Milky Way halo are used as an analog population representing the orbits of IMBHs. The 63 globular clusters with known position and velocity vectors are therefore used as initial conditions for the numerical orbit integration. Each time a globular cluster collides with a molecular cloud, the luminosity according to the Bondi-Hoyle accretion is calculated.
This represents the first step towards the investigation whether IMBHs can cause observable X-Ray luminosities or even ULXs via accretion in molecular clouds or not.

4.2 Molecular cloud distribution - 2D model

Although the number of IMBHs in the halo is unknown and their orbital motions require analogies as just described, the number and properties of molecular clouds to collide with can be approximated. Due to the lack of gas, molecular clouds are not to be expected outside the galactic disc. Consequently, only molecular clouds within the galactic disc are modeled. In this section, the probability for an object to hit a molecular cloud while passing through the galactic disc is derived.
The modeling process consists of following steps:

1. The molecular cloud distribution is axisymmetric around the galactic center. The midpoint of each cloud is located in the galactic disc (z = 0). The radial dependence of the distribution is derived using observations within the first galactic quadrant and extrapolating towards the complete disc.

2. The molecular cloud distribution is associated with a mass distribution. Using this and assuming a cloud density profile, the cloud radius distribution R_{cloud} is calculated.

3. Each molecular cloud is reduced into a flat, 2-dimensional circular object located within the galactic disc (z = 0). The surface area covered by the cloud is equal πR_{cloud}^2. The area coverage of all clouds is summed up, assuming no overlap between clouds, and divided by the total galactic disc area in order to obtain the fractional cloud coverage. As evidently following from step 1, this fractional cloud coverage is axisymmetric but changing radially.

4. The fractional cloud coverage equals the probability for an object to collide with a cloud while crossing the galactic disc. If a hit occurs, M_{cloud} of the hit cloud is derived in the way, that the overall cloud mass distribution is being followed. The speed vector of the cloud is determined by assuming that the cloud rotates in a perfect circular orbit within the galactic disc. From this point, the Bondi-Hoyle accretion is modeled as described in section 4.3.

The steps in detail:

Step 1

In order to obtain the spatial molecular cloud distribution, not the actual observed cloud distribution is used but instead the observed H_2 mass distribution. This follows the assumption mentioned in section 2.2, that about 90 % of the H_2 is indeed located in molecular clouds. The H_2 mass distribution, extrapolated from the first galactic quadrant towards the whole disc, is shown in figure 4 along with a triangle fit f(R). Note that the data points are binned: The data point located at radius R_i is the sum of the mass within the radius interval $[R_i - 0.25, R_i + 0.25]$, $R_i \in \{1.75, 2.25, ..., 15.75\}$. The fit function $f(R)$, although analytically, is also only evaluated at these discrete points (see step 3). Note that due to this discrete nature of $f(R)$,

$$\int_{R_i-0.25}^{R_i+0.25} f(R)dR = f(R_i) \tag{34}$$

According to Scoville & Sanders (1987), the relationship between the amount of observed molecular clouds N and their mass dM_{cloud} follows

$$\frac{dN_{cloud}}{dM_{cloud}} = c_R\ \alpha M_{cloud}^{\alpha-1} \tag{35}$$

with $\alpha = -0.61$. The proportional constant c_R depends on the total mass within the distribution. Since the total mass is given by $f(R)$:

$$M_{total}(R_i, R_j) = \int_{R_i}^{R_j} f(R)dR = \int M_{cloud}dN_{cloud} = \int_{M_{low}}^{M_{up}} \alpha c_R M_{cloud}^{\alpha} dM_{cloud} \qquad ; i < j \tag{36}$$

For a value of $\alpha = -0.61$, (36) and therefore the unknown c_R critically depends on the mass of the most massive observed molecular cloud M_{up} and the least massive, M_{low}. Hou et al. (2009) show in their figure 2 an upper mass of $2 \cdot 10^7 M_\odot$ and a lower mass cut-off at $M_{low} = 10^4 M_\odot$, which is used.
Solving the integral yields c_R:

$$c_R = \frac{\alpha + 1}{\alpha} \frac{M_{total}(R_i, R_j)}{M_{up}^{\alpha+1}} \tag{37}$$

Plugged into (35), the total number of clouds depending on R can be calculated:

$$N_{cloud} = \int dN_{cloud} = \alpha + 1 \frac{M_{total}(R_i, R_j)}{M_{up}^{\alpha+1}} \int_0^{M_{up}} M_{cloud}^{\alpha-1}\ dM_{cloud} \tag{38}$$

For the next step it is more convenient to use the differential form (35) rather than calculating the total number of clouds in each interval for R and afterwards assigning each cloud a statistically correct mass.

Step 2

In this step, a relationship between the mass of the molecular cloud M_{cloud} and its radius R_{cloud} (assuming a spherical symmetric cloud) is derived. The base of this derivation is the empirically found connection with proportional factor k between the 1-Dimensional velocity dispersion σ and the size of the cloud (Scoville & Sanders, 1987),

$$\sigma = k \left(2 \frac{R_{cloud}}{pc} \right)^{\beta} \ km\ s^{-1} \tag{39}$$

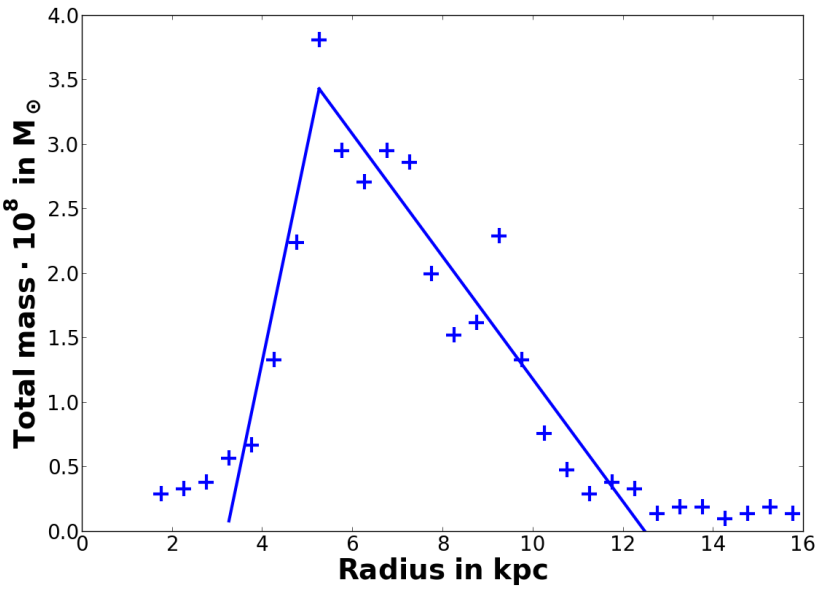

Figure 4: *The extrapolated total H_2 mass in the galactic disc versus the galactic radius. Crosses: data points from (Clemens et al. (1988), fig.11), solid line: fit of the data points.*

assuming a $\frac{1}{r}$ density profile within the cloud. The mass is then linked to the radius using the virial theorem: The theorem balances the gravitational potential energy of the particles with their internal kinetic energy via the radius of the cloud. The balanced state is called virial equilibrium; all clouds are assumed to be in virial equilibrium.
For simplicity, but taking into account the expected densed core within a self-gravitating system, the mentioned $\frac{1}{r}$ profile for the molecular clouds is used:

$$\rho(r) = C \cdot \rho_0 \cdot \frac{R_{cloud}}{r} \tag{40}$$

with $\rho(r)$ the density, ρ_0 the mean density of the cloud, r the distance from the cloud midpoint, and C a constant. The constant is linked with ρ_0 and M_{cloud}:

$$M_{cloud} = 4\pi \int_0^R r^2 \rho(r) dr = 2C\pi\rho_0 R_{cloud}^3 \tag{41}$$

Which requires $C = \frac{2}{3}$.
Assuming the cloud consists of N particles with equal mass m, the total kinetic energy T is given by

$$T = \frac{1}{2}\sum_{i=0}^{N} m_i v_i^2 = \frac{M_{cloud}}{2}\sum_{i=0}^{N}\frac{v_i^2\ m}{M_{cloud}} \tag{42}$$

Since

$$\langle v^2 \rangle = \frac{\sum_{i=0}^{N} v_i^2}{\sum_{i=0}^{N} 1} = \frac{\sum_{i=0}^{N} v_i^2 m}{\sum_{i=0}^{N} m} = \frac{\sum_{i=0}^{N} v_i^2\ m}{M_{cloud}} \tag{43}$$

the kinetic energy can be written as

$$T = \frac{M_{cloud}}{2}\langle v^2 \rangle = \frac{M_{cloud}}{2}\sigma^2 \tag{44}$$

Assuming the velocity dispersion is homogeneous in all spatial dimensions, $\sigma = (\sigma_{1D}, \sigma_{1D}, \sigma_{1D})$, and σ_{1D} is the observed 1-Dimensional velocity dispersion,

$$T = \frac{3M_{cloud}}{2}\sigma_{1D}^2 \tag{45}$$

The total potential energy U of the spherical cloud can be calculated by dividing the sphere into shells and successively removing the outer most shell while summing up the energy needed to do so. The energy dU needed to remove a shell of mass dM depends on the mass contained within the shell $M(r)$ according to the gravity law:

$$dU = -\frac{GM(r)\cdot dM}{r} = -\frac{G\frac{4\pi}{3}r^3\rho \cdot 4\pi r^2 \rho}{r}dr = -G\frac{16\pi^2}{3}\rho^2 r^4 dr \tag{46}$$

Using (40), the total energy can be calculated by integration:

$$U = \int dU = -\frac{4}{9}\frac{GM_{cloud}^2}{R_{cloud}} \tag{47}$$

The virial theorem for gravity connects the total potential energy with the total kinetic energy:

$$\begin{aligned} 2T &= -U \\ \rightarrow 3M_{cloud}\sigma_{1D}^2 &= \frac{4}{9}\frac{GM_{cloud}^2}{R_{cloud}} \\ \rightarrow R_{cloud} &= \frac{4}{27}\frac{GM_{cloud}}{\sigma^2} \end{aligned} \tag{48}$$

Plugging in (39) and using convenient units,

$$R_{cloud} = \frac{1}{2}\left(\frac{M_{cloud}}{781k^2 M_\odot}\right)^{\frac{1}{2\beta+1}} pc \tag{49}$$

which connects the total mass of a molecular cloud with its radius. The values k and β are found by fitting observations to (39). Scoville & Sanders (1987) report $k = 0.5$ and $\beta = 0.55$ which is used in this thesis. As an example, a massive cloud of $M_{cloud} = 10^6 M_\odot$ has a radius of 29 pc.

Step 3

The in step 2 found relation between mass and radius for the molecular cloud population can be used to calculate the total disc area covered by molecular clouds. This is done by projecting the 3-Dimensional clouds onto the two dimensional galactic disc (z = 0). The resulting total area is then given by

$$A = \int \pi R_{cloud}^2 dN_{cloud} \tag{50}$$

Plugging in (49),(35) and (37) the cumulative area function is given by (all masses in $M_\odot$):

$$\begin{aligned} A_{cum}(m, R_i, R_j) &= \frac{\pi}{4}M_{total}(R_i, R_j)\left(\frac{1}{781k^2}\right)^{\frac{2}{2\beta+1}}\frac{\alpha+1}{M_{up}^{\alpha+1}}\int_0^m M_{cloud}^{\frac{2}{2\beta+1}+\alpha-1}dM_{cloud}\ \ pc^2 \\ &= \frac{\pi}{4}M_{total}(R_i, R_j)\left(\frac{1}{781k^2}\right)^{\frac{2}{2\beta+1}}\frac{\alpha+1}{M_{up}^{\alpha+1}}\frac{1}{\alpha+\frac{2}{2\beta+1}}m^{\alpha+\frac{2}{2\beta+1}}\ \ pc^2 \end{aligned} \tag{51}$$

As pointed out in step 1, $M_{total}(R_i, R_j)$ is a discrete function with intervals $\Delta R = 0.5\ kpc$. This allows the simplification, that all clouds are located completely within one of the intervals, border effects between the intervals, such that some clouds are partially located in two intervalls, are neglected. The bigger the intervals, the more accurate is this simplification, but in turn the resolution of the fractional area coverage function $A_{fraction}$ reduces.

$$A_{fraction}(R_i) = \frac{A_{cum}(M_{up}, R_i, R_{i+1})}{\pi(R_{i+1} - R_i)^2} \tag{52}$$

This implicitly assumes, that no clouds are overlapping each other. This is justified by the evaluation of (52) shown in figure 5. The highest fractional area coverage around 5 kpc does not exceed 3%, overlapping is therefore unlikely. The plot illustrates a peak area coverage between 4 and 6 kpc. This is in this work called the molecular ring.

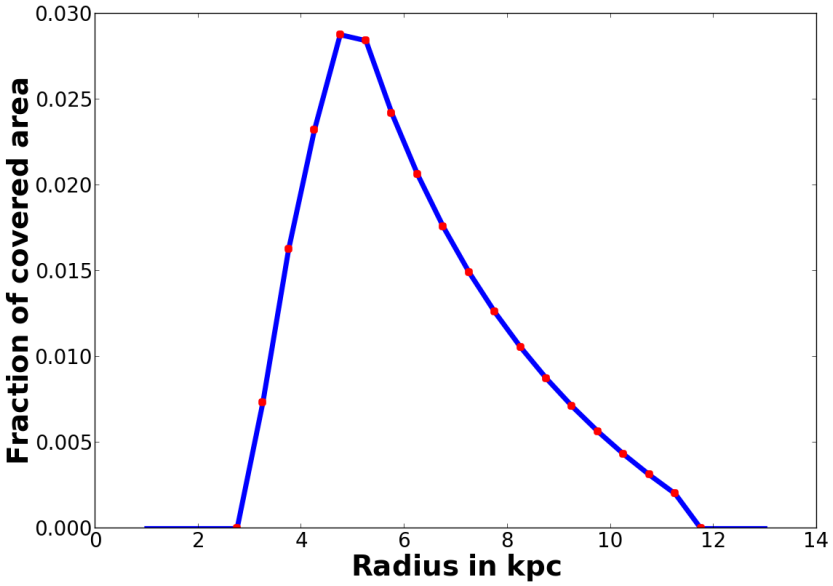

Figure 5: *Fraction of area covered by molecular clouds in the galactic disc as a function of galactic radius. Red circles: $A_{fraction}(R_i)$ versus R_i. Blue lines: linear interpolations.*

Step 4

If an object, (e.g. an IMBH) crosses during its orbit the galactic disc at the galactic distance R_{cross}, the fractional area coverage function is evaluated at $A_{fraction}(R_k)$ with $R_k \leqslant R_{cross} < R_{k+1}$. This represents the probability that a molecular cloud is hit. If a hit occurs, the mass of the hit molecular cloud is statistically derived from the normalized cumulated area function $A_{nc}(m)$:

$$A_{nc}(m) = \frac{A_{cum}(m, R_i, R_j)}{A_{cum}(M_{up}, R_i, R_j)} \tag{53}$$

Which implies $0 \leqslant A_{nc}(m) \leqslant 1$ (see figure 6). The mass is found by generating a random number $s \in [0, 1]$ and evaluating numerically the inverse function A_{nc}^{-1}:

$$M_{cloud} = A_{nc}^{-1}(s) \tag{54}$$

The velocity vector of the molecular cloud is derived by assuming the cloud orbits in a perfect circle around the galactic center at $R = \sqrt{x_0^2 + y_0^2}$ with x_0 and y_0 the coordinates of the object (IMBH)

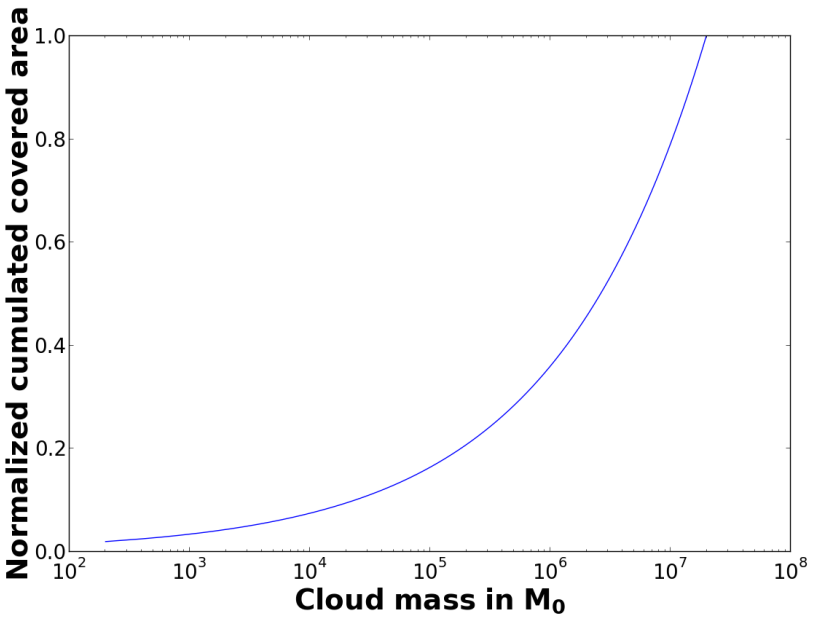

Figure 6: *Normalized cumulated surface area covered by molecular clouds* $A_{nc}(M_{cloud})$ *versus the cloud mass* M_{cloud}.

when the hit occurs. The circular velocity v_c is calculated using (11). The velocity vector of the cloud $v_{cloud} = (v_x, v_y, v_z)$ is then given as

$$\begin{aligned} v_x &= -v_c \frac{y_0}{R} \\ v_y &= v_c \frac{x_0}{R} \\ v_z &= 0 \end{aligned} \tag{55}$$

If

$$v_{IMBH} = (v_{x_0}, v_{y_0}, v_{z_0}) \tag{56}$$

is defined as the velocity vector of the IMBH at the collision point, then

$$v_{rel} = |v_{cloud} - v_{IMBH}| \tag{57}$$

is called the relative velocity between both objects.

4.3 Results

The orbits of the globular cluster population, the subset of globular cluster with known proper motions, has been numerically integrated for 10 Gyr. Each time a molecular cloud has been hit, the luminosity resulting from this event has been calculated.

4.3.1 Relative velocities

The relative velocity between the IMBH and the molecular cloud is a critical parameter in determining the Bondi-Hoyle luminosity, $L \propto \frac{1}{v_{rel}^3}$ (equation (26)). Due to the almost constant rotation curve (compare figure 1), this velocity barely depends on the distance R from the galactic center at which the cloud is hit, but is sensitive to the velocity vector of the IMBH. Both factors are determined by the shape of orbit of the IMBH (i.e. globular cluster).

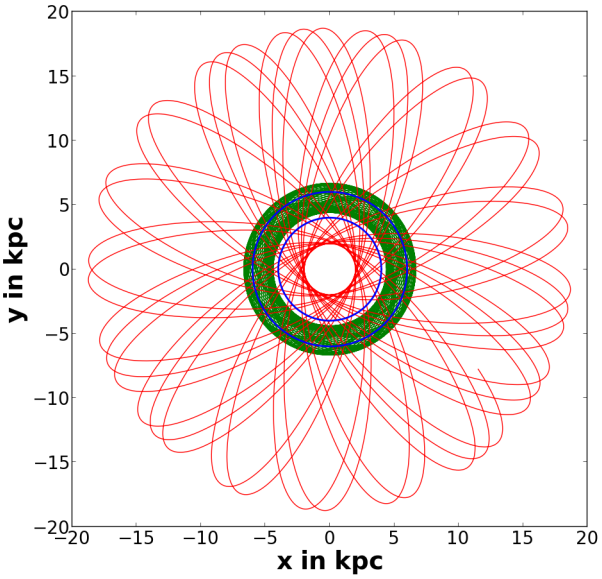

Figure 7: *Orbits of the globular cluster NGC 6838 (green) and 6553 (red) for 10Gyr in the x-y plane. The galactic center is at (x = 0, y = 0, z = 0). The blue circles indicate the border of the molecular ring.*

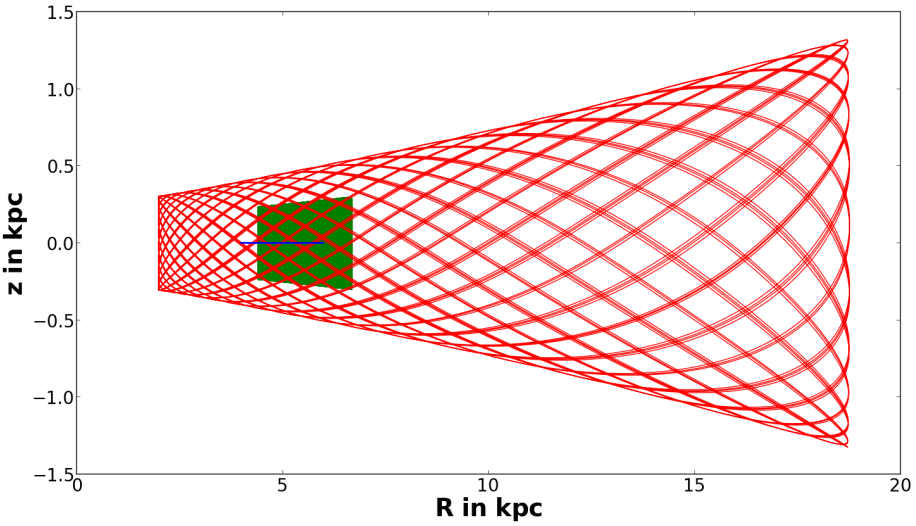

Figure 8: *Orbits of the globular cluster NGC 6838 (green) and 6553 (red) for 10Gyr.* $R = \sqrt{x^2 + y^2}$. *The galactic center is at (x = 0, y = 0, z = 0). The blue line indicates the molecular ring.*

Figure 7 and 8 illustrate the orbits for the globular cluster NGC 6838 and 6553. These plots give an overview about the general shapes of orbits within the Milky Way and the range of distances from the galactic center achieved.
While NGC 6838 is confined towards the galactic disc ($-0.4 < z < 0.4$) and forms a narrow ring around the galactic center, NGC 6553 goes deeper into the galactic halo and has a highly eccentric orbit. This two extreme examples illustrate, that the globular cluster population varies within a wide spread of orbital parameters. This in turn allows to draw general conclusions for halo-like IMBHs.
Ignoring the model described in section 4.2, figure 9 shows a histogram of the relative velocity for all globular cluster within the 10 Gyr integration time assuming that each time the galactic disc is crossed ($-100pc < z < 100pc$) a hit occurs.

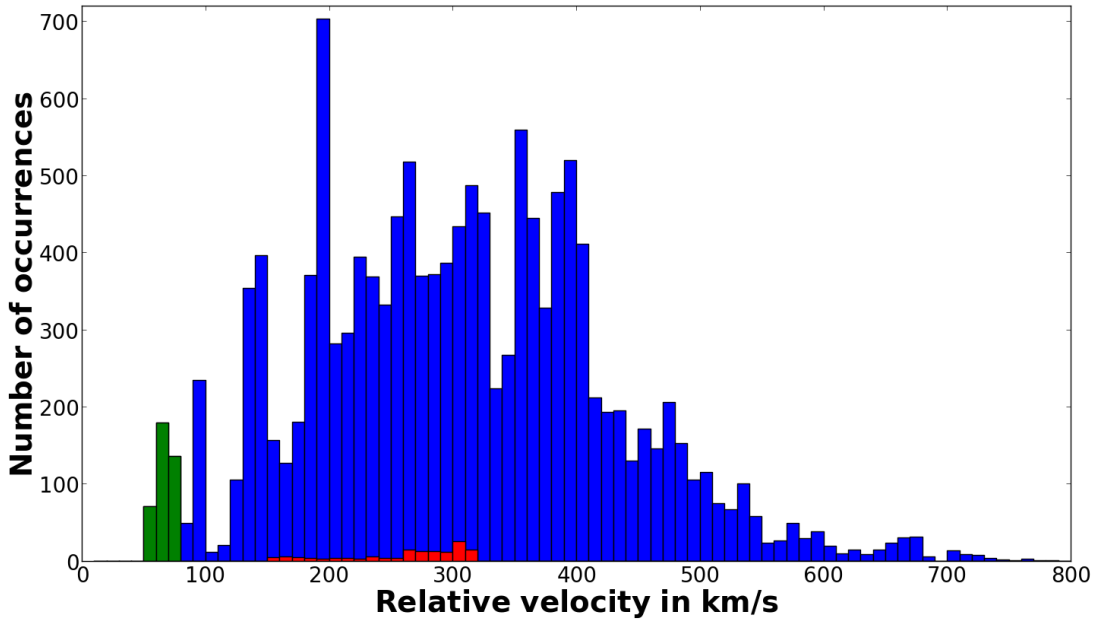

Figure 9: *Histogram of the relative velocities between globular clusters/IMBHs crossing through the galactic disc and a GMC orbiting in a perfect circular orbit according to the rotation curve, sampled for 10Gyr. It is assumed that each time the disc is crossed, a molecular cloud is hit. Green color: contribution of the globular cluster NGC 6838. Red: contribution of NGC 6553. Blue: total contribution of all globular cluster.*

The histogram visualizes, that the peak occurrence of relative velocities v_{rel} is about a few hundred km/s. According to figure 3, such high v_{rel} are not sufficient in order to produce ULX - luminosities of $L > 10^{39} \frac{erg}{s}$. Investigating the contribution of single globular cluster towards the total number of occurrences, following two statements can be made:

- The green color in the histogram indicates the contribution of the single globular cluster NGC 6838, it is therefore the only globular cluster which achieves $v_{rel} \leqslant 80 \frac{km}{s}$. The low relative velocities $< 100 \frac{km}{s}$ are statistically uncertain since only few objects realize them, leading to huge differences between similar v_{rel} in the histogram ranging from less than 10 to over 200 occurrence.

- Globular cluster which realize lower v_{rel} are over-representative in the histogram since their orbit shape, resulting in low v_{rel}, leads towards a higher frequency of disc crossings (compare figure 8). This is visualized by coloring the contribution of the globular cluster NGC 6553 in red; the total amount of disc crossings in the same time is significant lower for NGC 6553 than for NGC 6838.

In conclusion, orbit shapes of globular cluster which leads to high v_{rel} (about few $100\frac{km}{s}$) are far more common than orbit shapes for low relative velocities ($v_{rel} < 100\frac{km}{s}$). However, the mean relative velocity averaged over all low relative velocities is a uncertain quantity since these v_{rel} are only achieved by very few orbits, meaning too few examples are available in this regime for a meaningful statistic.

4.3.2 Collisions: Luminosity

As mentioned, figure 9 sets the probability of colliding with a molecular cloud while passing the disc to 100%. The described model in section 4.2, in which the probability to hit a cloud is determined by the fraction of disc area the whole cloud population covers, reduces the probability towards $0 - 3$ %, depending on the distance from the galactic center (see figure 5). This additionally adds a dependency on the orbital shape of the globular cluster, since only orbits within the molecular ring (4 -6 *kpc*) do have a reasonable chance of colliding with clouds. In order to visualize this, for each disc crossing the probability to hit a cloud is evaluated resulting into a total number of hit clouds per globular cluster within 10 Gyr. For most of the globular cluster the statistical noise is too high, meaning that the total number of disc crossings is too low to result into any or only few hits due to the low probability. In order to obtain a useful statistic representing the properties of the different orbits in general, the total number of hit clouds within the 10 Gyr is calculated 50 times with different sets of random variables which determine if a hit in a particular disc crossing occurred or not. The different results are then averaged. The top plot of figure 10 shows for each globular cluster on the ordinate the averaged number of hit clouds with its 1-σ error, the abscissa the mean distance from the galactic center when hits occur, also including the 1-σ error. The bottom plot shows on the ordinate the in the same way averaged v_{rel} for each globular cluster with its 1-σ error. The abscissa is identical to the top plot for easy comparison; the errorbar is here not shown for better clarity. The key results of both plots can be summarized as follows:

- The total number of hit clouds correlates tightly with figure 5: Only globular cluster orbits entering the molecular ring have a chance to hit several clouds within 10 Gyr.
- Most of the globular cluster have a spread in R of several kpc, meaning their orbits cross the disc at very different locations within the 10 Gyr.
- The relative velocities are not correlated with the entrance point R in the galactic disc. Although the data points pile up within the molecular ring, all different values for v_{rel} are realized, no general bias towards lower or higher values can be observed.

The next physical property needed to be taken into account is the mass distribution of the molecular clouds. Each time a hit occurs, the mass is statistically selected according to (54) and transformed into a mean gas density inside the cloud ρ_0 by (41). The luminosity, the quantity actually observable on earth and comparable to observations, is then calculated according to (26). Note here that the cloud is always assumed to be crossed through its full length $2R_{cloud}$ and the gas density during this crossing is constant (ρ_0). The mass of the IMBH is assumed to be $M_{BH} = 10^4 M_\odot$. The again over 50 sets of random variables (this time also effecting the random size of the molecular cloud in each hit) averaged luminosity is plotted in figure 11. The errorbars in luminosity are therefore determined by both the uncertainty of v_{rel} and M_{cloud}. However, no major fluctuation in the length of the errorbar compared to figure 10, bottom, can be observed, suggesting that the contribution and uncertainty of v_{rel} outweights that of the cloud mass M_{cloud}. This is not an unexpected result since the luminosity is proportional to $\frac{1}{v_{rel}^3}$ (equation (26)). This result can be qualitatively summarized as

- The luminosity is weakly sensitive towards M_{cloud} and very sensitive towards v_{rel}.

The last investigated property of the collisions is the shining time t_{sh} for each globular cluster, defined as the fraction of time spent within molecular clouds with respect to the total orbit time of 10 Gyr. This uses the assumption made section 3.2, that the bound gas molecules in the molecular cloud are instantaniously accreted, meaning the accretion luminosity is only produced as long as the IMBH is within the cloud. Additionally, to obtain a more realistic value, the oscillation in accretion mentioned in section 2.3 is taken into account. As described there, only in about 6 % of the total accretion time

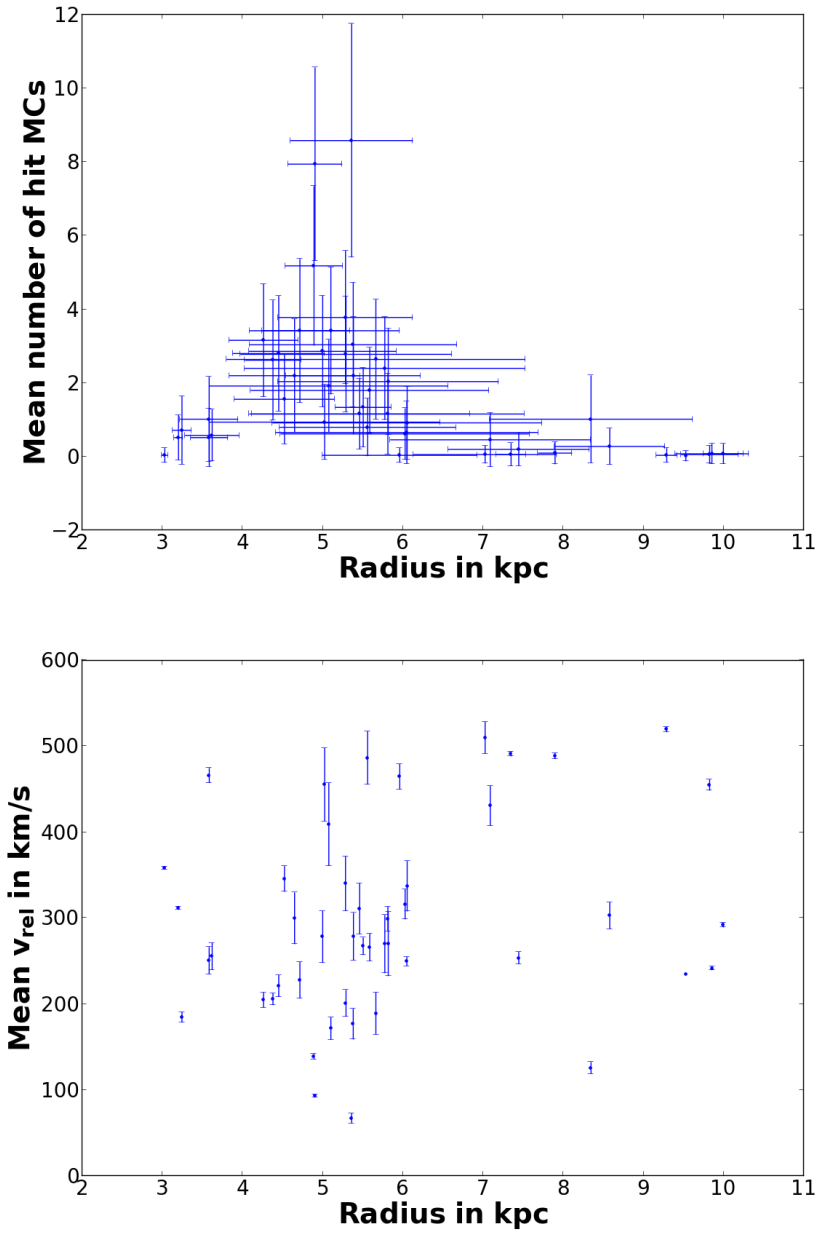

Figure 10: *Top: Total number of hit molecular clouds (MCs) per globular cluster after 10Gyr, averaged for 50 sets of random variables (see text) versus the mean distance R_{mean} from the galactic center while the hits occur. Bottom: corresponding mean relative velocities versus R_{mean}. Error bars indicate the 1-σ error.*

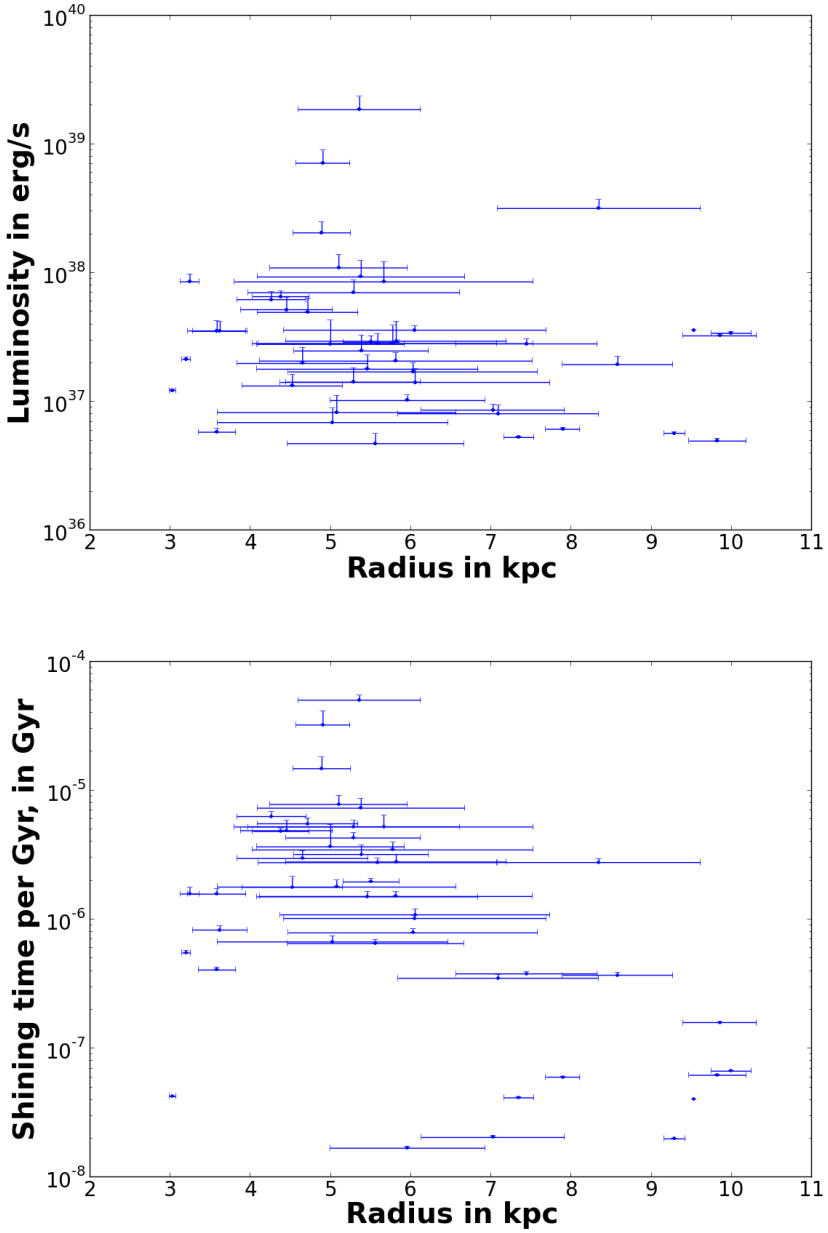

Figure 11: *Top: Mean luminosity while accreting within molecular clouds versus galactic radius for each globular cluster, assuming* $M_{BH} = 10^4 M_\odot$ *and averaged for 50 sets of random variables (see text) versus the mean distance* R_{mean} *from the galactic center while the hits occur. Bottom: Fraction of time spent in molecular clouds, reduced by* 94 *% due to accretion oscillations (see text), versus* R_{mean}*. Error bars indicate the 1-*σ *error.*

the peak luminosity is actually reached. This factor of 6 % is used here to scale the found shining time t_{sh} down accordingly. Figure 11, bottom, shows the result: Assuming that each globular cluster contains/is an IMBH then no IMBH is visible for more than 0.01 % of their orbit time or 0.1 Myr per 1 Gyr. The average shining time is $3 \cdot 10^{-6}$ years per year. Using this average, the following conclusion can be drawn:

- If it is assumed that a population of $3.3 \cdot 10^5$ IMBHs on similar orbits as the globular cluster orbits exists, statistically about $3.3 \cdot 10^5 \cdot 3 \cdot 10^{-6} = 1$ observable X-Ray source with luminosity $10^{36} \frac{erg}{s} < L < 10^{40} \frac{erg}{s}$ can be expected at any given time. (Assuming $M_{BH} = 10^4 M_\odot$)

5 Isotropic population

5.1 Overview

Based on the results from the globular cluster (section 4) which have been used as an analogon population for IMBHs, this section is dedicated to increase the number of objects and therefore to improve the statistics in terms of noise (compare the fluctuations of occurrences between similar v_{rel} in figure 9). This is done by creating a 'random' population based on the globular cluster orbital parameters. Since the globular cluster represent a population observable today, this approach allows to investigate a broad range of reasonable orbits. The general aim for this investigation is to derive a relationship between one or several orbital parameters and the expected relative velocities while crossing the disc.
The overall goals of this section are therefore defined as

- Obtaining a richer statistic for verifying or correcting the results from section 4
- Establishing a direct relation between orbital parameters and v_{rel}
- Predicting the lowest possible v_{rel} and corresponding parameters

The last point, the predictions, then finally lead into a more detailed investigation for especially interesting orbits in section 6.
The orbit integration technique, the accretion model and the molecular cloud distribution and therefore the collision probabilities and properties are unchanged compared to section 4.

5.2 Orbit creation

The first step towards creating randomized orbits in the 3-Dimensional Milky Way potential is to identify the orbital parameters most responsible for the resulting relative velocity v_{rel} (as defined in (57)). These parameters will then be randomized in order to create a new IMBH population.

The results from section 4 indicate, that the relative velocities are not correlated with the entry point R towards the galactic disc (compare figure 10, bottom). This can be rationalized as follows: The circular velocity of the molecular clouds (11) is close to independent of R in the region where hits can occur ($\approx 3 - 11$ kpc, compare figure 5), as seen in the rotation curve (figure 1). The variation in the cloud velocities is only of the order of about 10 % and can therefore not be responsible for the wide range of v_{rel} of several hundred $\frac{km}{s}$ (compare figure 9). The velocity of the IMBH ($|v_{IMBH}|$, the absolute of (56)) also does not directly depend on the entry point R but on the eccentricity e, defined as

$$e = \frac{r_{max} - r_{min}}{r_{max} + r_{min}}. \tag{58}$$

with r_{max} and r_{min} the maximum and minimum distance from the galactic center reached during the integration time. A low eccentricity implies a circular orbit, either in the galactic disc or outside, with lower and less varying velocities compared to high eccentricities; high eccentricities suggest falling into and again climbing the potential well which requires high absolute velocities. Therefore, e can be expected to be a critical orbital parameter in determining v_{rel}.
Another aspect is the angle of the entry point into the galactic disc. The molecular clouds are modeled as moving objects according to (55) rather than being static. Assuming the same $|v_{IMBH}|$, an entry into the disc perpendicular to the disc necessarily results into a different v_{rel} than with a with respect to the disc tilted trajectory. This suggests a "tilt angle" of the IMBH orbit with respect to the disc could be a parameter which is possibly responsible for a rich variation in v_{rel}. Such a "tilt angle" can be identified as the angle α, defined as the angle between the angular momentum vector J,

$$J = (J_x, J_y, J_z) = x \times v \tag{59}$$

of the IMBH at the time t_J and the z = 0 axis of the coordinate system:

$$\alpha = \arccos\left(\frac{J_z}{|J|}\right) \tag{60}$$

$J_z > 0$ corresponds to $0° \leqslant \alpha < 90°$ and implies an orbit of the same sense of rotation as the molecular clouds in section 4.2. This is in this work referred to as a positive rotation. $\alpha = 0°$ defines a positive rotation within the galactic disc. $J_z < 0$, meaning $90° < \alpha \leqslant 180°$, corresponds to a negative rotation against the disc.
Note that due to the cylindrical symmetry of the potential, only J_z rather than J is a conserved quantity over time. Therefore, for a comparability between orbits, t_J is chosen to be the time in which the object within its integration time of 10 Gyr reaches the maximum distance from the galactic center:

$$r(t_J) = \max(r(t)) \equiv r_{max} \tag{61}$$

Closely related is the maximum height z_{max} the orbit reaches above/under the disc. An object starting at high z accelerates longer towards the galactic disc, resulting in high $|v_{IMBH}|$ in the disc, and then deaccelerates after passing the disc until $v_z = 0$ is reached at the turning point (compare figure 8). This is directly analog towards a 1-Dimensional spring, only complicated due to the 3-Dimensional movement. Although this effect is expected to influnce v_{rel}, z_{max} and α for constant J are directly correlated (increasing height for increasing α up to $\alpha < 90$, decreasing height for $\alpha > 90$), so that both quantities do not need to be treated separately in the investigation of the v_{rel} dependency.
In conclusion, e and α are expected to be the main contribution in determining v_{rel}.

As a first step, the orbits are randomized in α; it will turn out that this procedure together with the chosen boundary conditions also creates a useful variety in e. The random orbits are required to be realistic and a natural extension of the globular cluster orbits in the sense, that the distances from the galactic center r and the absolute of the angular momentum J are within the same value range as for the globular cluster orbits. This implies the identification of globular cluster orbits with IMBH orbits, as already done in section 4. In detail, the following steps for each globular cluster individually are taken in order to create in α randomized orbits. Steps 2 - 4 are explained in detail below.

1. Within the 10Gyr integration time of the globular cluster, the values r_{min} and r_{max}, the minimum and maximum distance from the galactic center, are determined.
2. The globular cluster orbit is projected onto the galactic disc.
3. A random distribution of the angle α is determined.
4. The projected, flattened orbit from step 2 is tilted using α.

The steps 2-4 in detail:

Step 2

Projection onto the galactic disc:
An orbit is searched with $z(t) = 0$ for all times t and the same values for r_{min} and r_{max} as for the globular cluster orbit. To find initial conditions satisfying these requirements, the coordinate system is rotated [2] in the way that

$$r_{max} = r(t_p) = \sqrt{x(t_p)^2 + y(t_p)^2 + z(t_p)^2} = x(t_p) = x_{max} \tag{62}$$

meaning the turning point of the orbit at time t_p is on the x-axis.
From this follows $v_x(t_p) = 0$ since $\dot{r}(t_p) = 0$.

[2] Due to the rotation symmetry of the potential, the physical properties including the resulting v_{rel} are invariant for rotation within the x-y plane

$v_y(t_p)$ is determined by demanding $\min(r(t)) = r_{min}$:
An initial guess for v_y is used and the resulting orbit with initial conditions as in (63) is integrated for 2 Gyr. The resulting minimum distance towards the galactic center, r'_{min}, is compared to the desired r_{min}. A new initial guess based on the result is calculated and the procedure repeated. If $\Delta r_{min} = |r'_{min} - r_{min}| < 0.01pc$, then the corresponding $v_y(r'_{min})$ is accepted. The initial conditions for the flattened orbit are therefore:

$$\begin{aligned} x(t_p) &= r_{max} & v_x(t_p) &= 0 \\ y(t_p) &= 0 & v_y(t_p) &= v_y(r'_{min}) \\ z(t_p) &= 0 & v_z(t_p) &= 0 \end{aligned} \tag{63}$$

Step 3

Random angle α:
Let ρ be the angle between the onto the x-y plane projected angular momentum vector J and the x-axis, $\tan(\rho) = \frac{J_y}{J_x}$. Then $\rho \in [0, 2\pi]$ and $\alpha \in [0, \pi]$ define a point on the surface of a sphere. Since the area element dV is a function of α, $dV = \sin(\alpha) d\alpha d\rho$, picking random numbers from the intervals $[0, 2\pi]$ and $[0, \pi]$ for ρ and α, respectively, will result in a point distribution biased towards the poles.
Therefore, the points need to be picked following the distribution $\sin(\alpha)$:

$$c \int_0^{\alpha} \sin(\alpha) d\alpha = y \equiv F(\alpha) \tag{64}$$

with y a random variable picked from the interval $[0, 1]$ and c the normalization constant.
Normalization towards the interval $[0, 1]$:

$$\begin{aligned} 1 \stackrel{!}{=} F(\pi) &= c\ (-\cos(\pi) + \cos(0)) = 2c \\ \Rightarrow c &= \frac{1}{2} \end{aligned} \tag{65}$$

Inverting $F(\alpha)$ results in

$$\begin{aligned} F(\alpha) &= \frac{1}{2}[-\cos(\alpha) + 1] = y \\ \Rightarrow \alpha &= \arccos(1 - 2y) \end{aligned} \tag{66}$$

This transforms the random number y into a correctly distributed random number α. For each globular cluster orbit, 20 random numbers for α are determined.

Step 4

Tilt of the projected globular cluster orbit with α:
If the index t refers to the tilted orbit constructed in this step and the index f to the flat orbit of the projected globular cluster from step 2, then the initial conditions for an orbit which is satisfying in at least one point

$$|J_t| = J_{z,f} \tag{67}$$

is searched. This conservation of angular momentum loosely ensures that the values $r_{min,t}$ and $r_{max,t}$ are similar compared to the ones from the flat orbit and enable in a simple manner the tilting of the orbit itself. The angular momentum vector is then readily constructed as

$$\begin{aligned} J_{x,t} &= J_{z,f} \cdot \sin(\alpha)\ \cos(\rho) \\ J_{y,t} &= J_{z,f} \cdot \sin(\alpha)\ \sin(\rho) \\ J_{z,t} &= J_{z,f} \cdot \cos(\alpha) \end{aligned} \tag{68}$$

In the same point as in step 2, namely $y = 0$, $z = 0$, $v_x = 0$ and $x = r_{max,f}$, the position and velocity vectors can now be constructed using (59) and (68):

$$J_{z,t} = x\ v_y - y\ v_x \qquad J_{y,t} = z\ v_x - x\ v_z \qquad J_{x,t} = y\ v_z - z\ v_y = 0$$
$$\Rightarrow v_y = \frac{J_{z,t}}{x} = \frac{J_{z,t}}{r_{max,f}} \qquad \Rightarrow v_z = -\frac{J_{y,t}}{x} = -\frac{J_{y,t}}{r_{max,f}} \qquad \Rightarrow cos(\rho) = 0 \ \Rightarrow \rho = \frac{\pi}{2}$$

This procedure implies, that each constructed orbit has a turning point with $\dot{r} = 0$ in the x-y plane. For each globular cluster, 20 of such in α randomized orbits are created.

5.3 Results

5.3.1 Comparison with globular cluster

As listed in section 5.1, the first goal of the random population is to provide a natural extension of the globular cluster population with the purpose of verifying the statistics. This section is dedicated to re-evaluate the results made in section 4.

The total number of disc crossings for all 63 globular cluster is $N_{GC} = 13764$ (total area in figure 9), the total number for all $63 \cdot 20 = 1260$ random orbits is $N_R = 335299$, meaning the average number of disc crossings per object n_{cross} increases in the random population by 22 %. This discrepancy is plausible by analyzing figure 12. Figure 12 shows a histogram of the relative velocities while crossing the disc for all objects of the globular cluster population (blue, same as figure 9) and the random population (red). The total number of crossings in each bin for the random population are reduced by the factor $\frac{N_R}{N_{GC}} = 24.3$ in order to make both populations comparable by forcing the total area of the histograms to be equal.

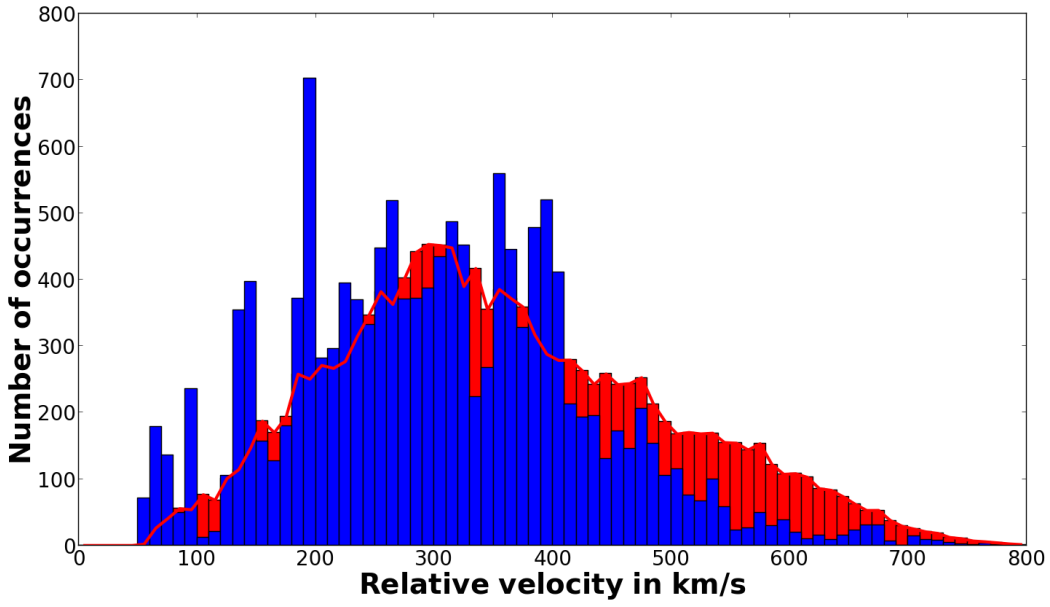

Figure 12: *Histogram of the relative velocities while passing through the galactic disc. Blue: Globular cluster population (63 objects), red: random population created according to section 5.2 (1260 objects). The numbers for the random population are scaled down in a way that the total number of collisions for both populations is identical. The red curve highlights the peaks of the random population since they are in some cases covered by the blue bars.*

The random population is as expected and intended far less noisy than the globular cluster population with a peak at $300km/s$. The distinct local peaks of the globular cluster population at $360-400km/s$, $180-200km/s$ and $130-150km/s$ and the structure below $100km/s$ are not reproduced and can therefore be attributed to noise due to the low number of globular cluster. Therefore, also n_{cross} is expected to be influenced by the inhomogeneity.
The region for v_{low} ($v_{low} < 100\ km/s$) is not longer produced by one single object (compare figure 9, green bars) which evidently overrepresented these velocities. The peaks are smoothed out and blend into the overall distribution.
In the region above $400km/s$ the random distribution is permanently in excess of the globular cluster distribution, meaning the orbit parameters of the latter case responsible for these velocities are underrepresented.
However, the similarity and therefore comparability between both populations is limited. The most systematical discrepancy found is the eccentricity e (58). Figure 13 plots as an example for the problem the minimum and maximum distance r_{min} and r_{max} from the galactic center within the 10 Gyr integration time for the 20 random objects based on the globular cluster NGC 1904 versus the maximum height z_{max} above the galactic plane. The red line represents the values for the globular cluster itself. Although r_{max} stays constant and equals the globular cluster case for all random objects, r_{min} is decreasing with increasing z_{max}. Since r_{max} and r_{min} of the globular cluster equal by design the case of the flattened orbit with $z_{max} = 0$, the random orbits are not able to reproduce the eccentricity of globular cluster with high z_{max}.

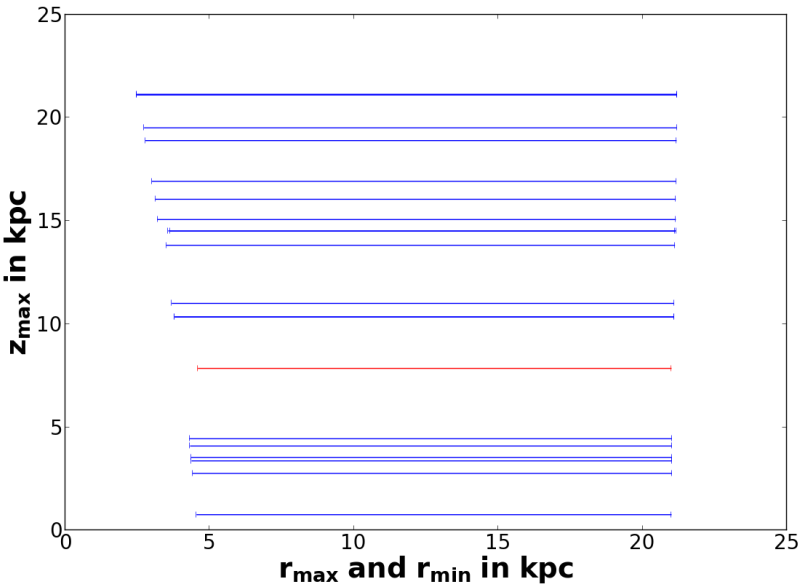

Figure 13: *Maximum height above the plane z_{max} versus the minimum (r_{min}) and maximum (r_{max}) distance from the galactic center within 10 Gyr. Blue: The 20 random orbits based on the globular cluster NGC 1904, red: The globular cluster itself.*

Assuming each object is a black hole of $M_{BH} = 10^4 M_\odot$, the mean luminosities calculated for each object reach only in 9 cases (out of 1260) $10^{39} < L < 10^{40}\,\frac{erg}{s}$ due to still too high minimum v_{rel} of not lower than $50\frac{km}{s}$ (see figure 12).
The mean shining time, defined as in section 4 as the time spent within clouds divided by the whole simulation time of 10 Gyr and times the factor 0.06 for taking into account oscillations in the accretion, averaged over all 1260 objects, is $1.9{\cdot}10^{-6}$, therefore slightly lower than in the globular cluster population. Assuming then $5.3 \cdot 10^5$ IMBHs are orbiting on orbits similar to the orbits of the random population,

then on average, $5.3 \cdot 10^5 \cdot 1.9 \cdot 10^{-6} = 1$ X-Ray object can be expected to be visible at any given time in the Milky Way ($10^{36} \frac{erg}{s} < L < 10^{40} \frac{erg}{s}$). For having one ULX with $10^{39} \frac{erg}{s} < L < 10^{40} \frac{erg}{s}$ permanent visible, $1.1 \cdot 10^7$ IMBHs are necessary.
Concerning the first general goal of the random population as described in section 5.1, the results so far can be summarized as:

- The random population extends the globular cluster population with systematically differing eccentricity in the sense, that in the random population r_{min} decreases with increasing z_{max} within one set of orbits based on the same globular cluster. The actual globular cluster value for z_{max} and r_{min} might therefore not be represented.

- Within this limitation, the random population produces a smoothed version of the globular cluster relative velocity distribution.

- With the constraint that relative velocities $v_{rel} < 100 \frac{km}{s}$ are uncommon and blend neatly into the overall distribution, all conclusions made in section 4 remain valid. The number of IMBHs necessary to create one visible X-Ray source at any given time increased from $3.3 \cdot 10^5$ to $5.3 \cdot 10^5$.

5.3.2 Relation between α, e and v_{rel}

The orbit creation in section 5.2 assumed, that the most critical parameters influencing v_{rel} are the inclination of the orbit α (60) and the eccentricity e (58). According to the goals of section 5.1, this section empirically derives the relation and enables predictions for v_{rel}.

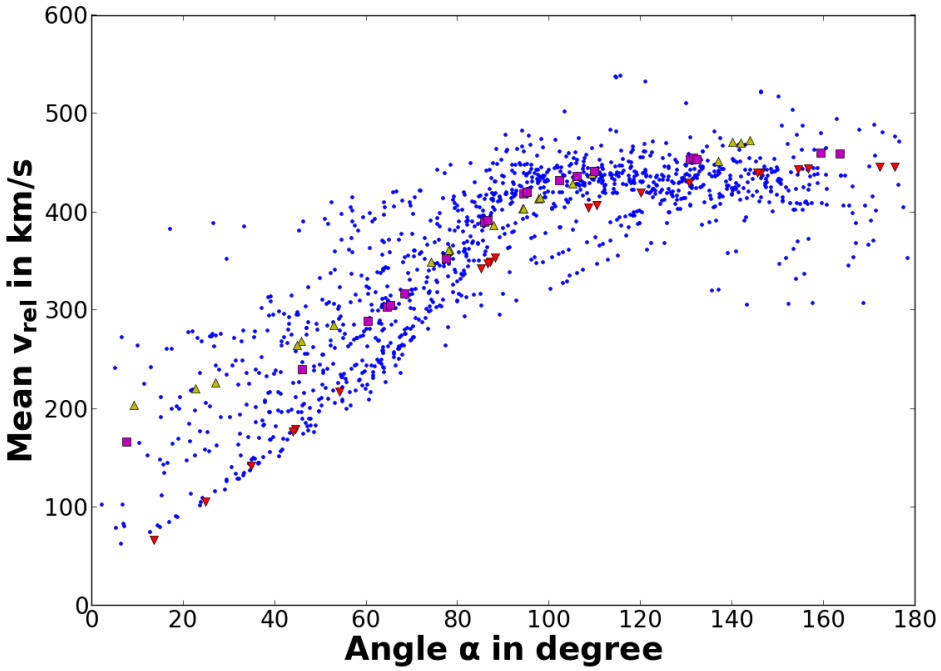

Figure 14: *The mean relative velocity while passing the galactic disc for each of the 1260 random orbits versus the initial inclination angle α. The random orbits based on the globular cluster NGC 104 (red downwards triangles), NGC 1851 (yellow upwards triangles) and NGC 2298 (magenta squares) are highlighted.*

For each random orbit, 1260 in total, the mean relative velocity $\bar{v}_{rel}$ resulting from collisions with molecular clouds while passing the galactic disc is calculated. For the sake of a more accurate statistic, it is assumed that each disc crossing has a hit probability of 100 %. The mean relative velocity $\bar{v}_{rel}$ is plotted versus the random inclination angle α in figure 14. The data points for the orbits based on the clusters NGC 104, NGC 1851, NGC 2298 are highlighted in order to emphasize the trend within one set of orbits. For $\alpha > 90°$, implying a negative rotation compared to the sense of rotation of the molecular clouds, $\bar{v}_{rel}$ saturates towards $\approx 440\frac{km}{s}$, which equals about twice the rotation velocity of the disc (figure 1). This corresponds to the relative speed resulting from the collision of two objects circling with a opposite sense of rotation within the disc on circular orbits. For orbits with a positive sense of rotation, $\bar{v}_{rel}$ shows a systematic relation with the inclination angle α; lower inclinations correlate with lower $\bar{v}_{rel}$. Additionally, lower inclinations result in higher spreads in $\bar{v}_{rel}$. For values $\alpha < 20°$, $\bar{v}_{rel}$ reaches its minimum of about $60 - 100\frac{km}{s}$ for few orbits, but the spread reaches up to $280\frac{km}{s}$.
The marked data points, identifying the results of the 20 random orbits based on the same globular cluster, follow very strictly a monotonous decreasing curve for decreasing angles. This strongly suggest a direct explicit relation between $\bar{v}_{rel}$ and α. Since such a relation necessarily depends on the complicated Milky Way potential, the existence of an analytical closed form is unlikely. Given the high density of data points, such an expression or a fit of the curve are unnecessary. Although each point on a curve for a given globular cluster basis is defined solely by the inclination angle, the difference between the curves for different globular cluster imply the influence of at least one further parameter. This parameter is identified as the eccentricity e.
Figure 15 displays a plot of e versus $\bar{v}_{rel}$ within the narrow range of $0° < \alpha < 20°$ for the inclination. A clear trend connects high eccentricities with high $\bar{v}_{rel}$, as motivated in section 5.2. The differences in the

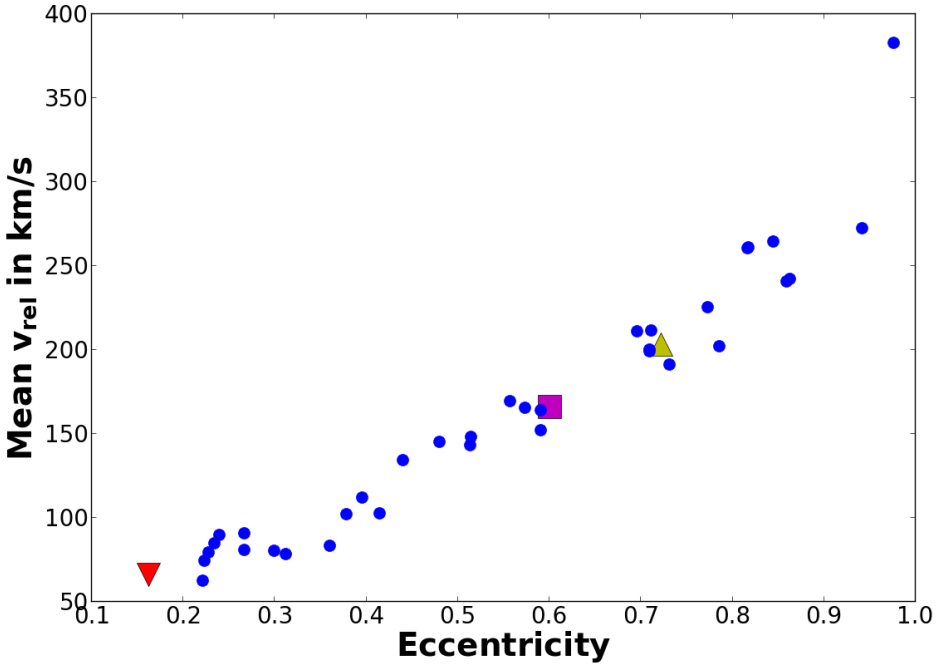

Figure 15: *The mean relative velocity while passing the galactic disc for all random orbits with initial inclination angle of $\alpha < 20°$ versus the orbit eccentricity. Symbols as in figure 14.*

curves are therefore plausible explainable via their differences in their eccentricities. It is nevertheless surprising, that eccentricities up to 0.4 are possibly able to create the lowest measured $\bar{v}_{rel}$. This enables for example an IMBH to cover within its low inclined orbit the molecular ring down to $r_{min} \approx 4kpc$ and spreading outwards towards $9kpc$ while achieving $\bar{v}_{rel} < 100\frac{km}{s}$.

In conclusion, the results of the random population based on globular cluster can be summarized as follows:

- The mean relative velocity $\bar{v}_{rel}$ depends directly on the the inclination α of the orbit with respect to the disc and its eccentricity e.
- $\bar{v}_{rel} < 100 \frac{km}{s}$ are achievable for disc-like orbits, defined as $\alpha < 20°$ and $e < 0.4$

Therefore, in order to create luminosities in the scope of ULXs, only disc-like orbits are possible candidates. However, a closer investigation using the 2D molecular cloud model as presented in section 4.2 becomes for this special case problematic. This is further addressed and solved in section 6.

6 Thin disc IMBHs

6.1 Overview

The statistically robust results from section 5 clearly indicate, that $v_{rel} < 100\frac{km}{s}$ and therefore luminosities of the order of ULXs (compare figure 3) are only reliable achievable for IMBHs with disc like orbits. This section investigates the possible impact of such IMBHs in three steps:

- Changing the molecular cloud model to fit the special case of orbiting within the disc
- Giving a theoretical motivation for the existence and number of IMBHs in the disc
- Comparing the resulting luminosity distribution with observable X-Ray sources

6.2 Molecular clouds - 3D Model

The 2D model for the molecular cloud distribution as described in section 4.2 does not hold for the case of orbits with too small inclinations α for two reasons:

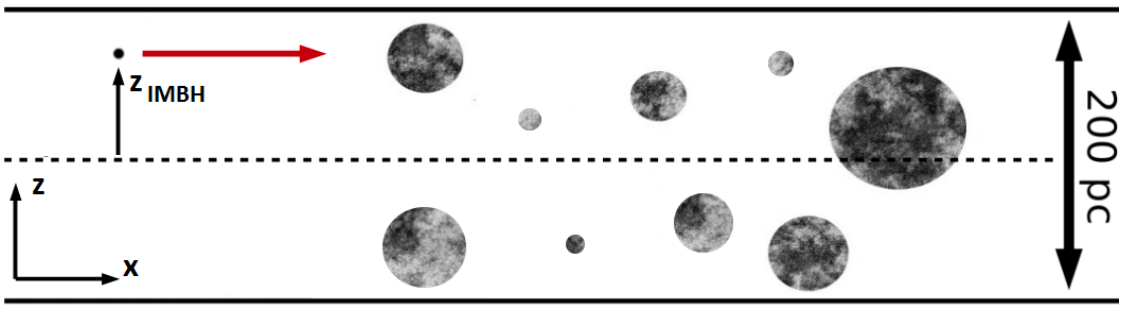

Figure 16: *Edge-on sketch of the galactic disc visualizing the problem for disc-like orbits. Coordinate system in the lower left corner; the dashed line indicates $z = 0$. The height of the disc is approximately 200 pc. The radius of the molecular clouds (gray shaded balls) is in the order of pc to several tens of pc. The Bondi-Hoyle radius for an IMBH with $M_{BH} = 10^4 M_\odot$ is 0.009pc (black circle at height z_{IMBH}, not to scale, otherwise it would be invisible). The red arrow indicates the direction of travel for the IMBH. The molecular cloud distribution in z-direction becomes evidently important since it influences if a hit occurs or not.*

First, in the 2-D model the molecular clouds have been assumed to be flat objects located in the x-y plane. This is an accurate model for IMBHs crossing the disc perpendicular, the deviation of the cloud from $z = 0$ up to about $z = 100pc$ is negligible and does not effect the question whether or not the cloud is hit. IMBHs orbiting parallel to the disc at a certain height z_{IMBH} might or might not hit certain molecular clouds depending on their location in z-direction (figure 16). Therefore, in the latter case the simplifying 2-D model can not be used.
Second, the 2-D model assumes a static distribution of molecular clouds; only after a hit occurred the theoretical speed of the cloud assuming a circular orbit is calculated. In the case of orbits in the disc (figure 16) the relative speed between clouds and IMBH becomes already important in determining the probability of a hit. For example, an IMBH following a molecular cloud in the very same circular orbit can never hit the cloud or any other cloud. This effect has been neglected in the 2-D model but needs to be taken into account for disc-like orbits.

In order to overcome the shortcomings of the 2-D model, in the thin disc simulation presented in this section all molecular clouds are treated as individual objects which are integrated forward in time analog to the IMBHs orbits according to (8). The statistical total number N of molecular clouds present in

the disc today can be calculated using (38) with $M_{total} = 1.6 \cdot 10^9 M_\odot$, the H_2 mass of the whole disc, and results in $N = 5227$ molecular clouds.

The radial distance $R = \sqrt{x^2 + y^2}$ from the galactic center for each cloud is determined by inverting the normalized cumulative function $N_{nc}(R)$ based on (38) (compare the analog situation for masses in (53), (54))

$$N_{nc}(R) = \frac{(\alpha+1)}{5227} \frac{M_{total}(0,R)}{M_{up}^{\alpha+1}} \int_{10^4}^{M_{up}} M_{cloud}^{\alpha-1} \, dM_{cloud} \tag{69}$$

The angular position of each molecular cloud is determined by a random variable $\rho \in [0, 2\pi]$,

$$\begin{aligned} x &= R \ \cos(\rho) \\ y &= R \ \sin(\rho) \end{aligned} \tag{70}$$

The distance z from the galactic disc is modeled via a normal distribution $f(z)$ with maximum at z = 0 and a standard deviation of $H = 100pc$,

$$f(z) = \frac{1}{\sqrt{2\pi}H} \ e^{-z^2/2H^2} \tag{71}$$

The normalized cumulative function $f_{nc}(z)$ is then

$$f_{nc}(z) = \frac{1}{\sqrt{2\pi}H} \int_{-\infty}^{z} e^{-z'^2/2H^2} \ dz' \tag{72}$$

Although the integral has no closed analytical form, it can be evaluated and inverted numerically. The inverted function then results for random variables $s \in [0, 1]$ into statistically correctly distributed values for z.
The initial velocity of each cloud is calculated according to (11). Note that due to the deviations from a flat orbit ($z \neq 0$ in general) the orbit becomes eccentric.
In order to simulate the finite empirical lifetime of molecular clouds of about $10Myr$, all molecular clouds are removed in $10Myr$ intervals from the simulation and are immediately replaced by an equal numbered population, again distributed as described above. Due to the different random variables in both populations, the overall distribution remains constant, but individual clouds vanish and reappear at different locations, simulating in a simple approximation the dynamics in the galactic disc.

6.3 Existence and number of IMBHs in the galactic disc

As mentioned in section 2.6, numerical simulations of stars in dense star cluster indicate, that IMBHs may form within about a few Myr by subsequent star/black hole collisions and merging in the core, i.e. in the bottom of the potential well of the cluster. Although the lifetime of the cluster itself does in most cases not exceed 100 Myr (Whitmore, 2009), the IMBH, once formed, can be expect to be present in the disc until today. The mass M_{BH} of the resulting IMBH is expected to be proportional to the total cluster mass, M_{cls} and ranges between

$$\begin{aligned} M_{BH} &= 2 \cdot 10^{-3} M_{cls} && \text{(Freitag et al., 2006)} \equiv Case\ A \\ M_{BH} &= 4 \cdot 10^{-2} M_{cls} && \text{(Portegies Zwart \& McMillan, 2002)} \equiv Case\ B \end{aligned} \tag{73}$$

Demanding $M_{IMBH} > 100 M_\odot$, this limits the mass of cluster capable of creating IMBHs to

$$\begin{aligned} M_{cls} &> 50000 M_\odot && (Case\ A) \\ M_{cls} &> 2500 M_\odot && (Case\ B) \end{aligned} \tag{74}$$

The total number of cluster which fulfil this mass boundary created during the lifetime of the Milky Way gives a first approximation for the number of IMBH possibly present in the disc today resulting from this mechanism. For the purpose of calculating this number, it is assumed that the star formation rate s_r in the history of the Milky Way is a constant and equals the value found today, $s_r = 3\frac{M_\odot}{year}$ (Misiriotis et al., 2006), and all stars are created within star cluster. The empirical relation between number of star cluster N_{cls} and their mass observed today follows (Lada & Lada, 2003)

$$\frac{dN_{cls}}{dM_{cls}} = \gamma M_{cls}^{-2} \tag{75}$$

With γ a constant. Given a total lifetime of the Milky Way of about $10^{10} yr$ (Chiappini et al., 2013), then the total star mass in the Milky Way is $3 \cdot 10^{10} M_\odot$, which equals the total mass of all cluster:

$$3 \cdot 10^{10} M_\odot = \int M_{cls} \cdot dN_{cls} = \int_{M_{min}}^{M_{max}} \gamma M_{cls}^{-1} dM_{cls} \tag{76}$$

This integral critically depends on M_{min} and M_{max}, the minimum and maximum possible mass of a star cluster. Here, two different values for M_{min} found in literature are used, $M_{min,1} = 20 M_\odot$ (Lada & Lada, 2003), $M_{min,2} = 50 M_\odot$ (Piskunov et al., 2008), in order to show the impact on the results if the number of heavy star cluster is lower (index 1) or higher (index 2). Also, M_{max}, the highest theoretically achievable cluster mass, is a difficult to be determined, but has, as shown in the results, no severe impact on the IMBH mass distribution. As following from the power law, more massive cluster are lower in number, therefore in principle less likely to be detected. Therefore, it is not sufficient to use the highest in the Milky Way observed cluster mass of $M_{max} = 4 \cdot 10^4 M_\odot$ as reported in Portegies Zwart et al. (2010) in their figure 2. Instead, the sample has to be increased by including nearby spiral galaxies. A fit of the cluster mass function towards such a sample done by Dowell et al. (2008) results into an upper mass of $M_{max} = 10^{7.5} M_\odot$, which is used here.
The integral then results for γ into

$$\begin{aligned} \gamma_1 &= 2.1 \cdot 10^9 M_\odot \\ \gamma_2 &= 2.2 \cdot 10^9 M_\odot \end{aligned} \tag{77}$$

With this, using (75) the total number N of clusters which possibly produced IMBHs can be calculated (which neglects the time needed to form the IMBH in the cores of ($\approx$ few Myr)):

$$N_{(1,2)} = \int dN = \int_{M_{(A,B)}}^{M_{max}} \gamma_{(1,2)}\ M_{cls}^{-2}\ dM_{cls} \tag{78}$$

The indices are defined as follows: The different considered lowest observed cluster mass create two scenarios labeled with index 1 and 2. Additionally, the two different cases which refer to different lowest possible cluster mass which still enables IMBH formation in the core create two more scenarios, labeled A and B. Combined, this results in 4 setups labeled $(A,1),\ (A,2),\ (B,1),\ (B,2)$ respectively. A notation $X_{(1,2)}$ or $X_{(A,B)}$ indicates that the value for X corresponding to the desired scenario needs to be plugged in.
$M_{(A,B)}$ refers to the lowest possible cluster mass for creating an IMBH inside the core for the different cases (see (74)). Evaluating (78) yields the total number of cluster which can create IMBHs for these four setups:

Case A	*Case B*
$N_{(A,1)} = 41934$	$N_{(B,1)} = 839934$
$N_{(A,2)} = 43930$	$N_{(B,2)} = 879930$

(79)

The mass of each cluster is individually determined by inverting the normalized cumulative function $N_{cum}(m)$; this procedure results in a cluster mass distribution which follows (75). Compare for details

the analog situation for the molecular cloud masses in (53) and (54).

$$N_{cum}(m) = \frac{\int_{M_{(A,B)}}^{m} M_{cls}^{-2}\, dM_{cls}}{\int_{M_{A,B}}^{10^{7.5}} M_{cls}^{-2}\, dM_{cls}} \tag{80}$$

The total mass of all IMBHs formed within cluster, assuming all cluster capable of creating IMBHs indeed do so, equals 1.1% of the mass of the Milky Way for setup (A,1) and 1.2% for setup (A,2). For setup (B,1) this equals 29.5%; for (B,2), 30.9%.

The spatial distribution is set to be identical to the molecular cloud distribution as presented in section 6.2. This follows the reasoning, that the molecular clouds eventually collapse into star cluster and inherit their orbit parameters. Note that the transition from molecular clouds into a star cluster is not modeled here; as described in section 6.2, all molecular clouds vanish and reappear from the simulation after a lifetime of 10 Myr. In contrast to that, the disc is only once populated with the in (79) defined number of IMBHs.

6.4 Results

This section presents the results following from integrating the molecular clouds and the IMBHs located within the thin disc for 10 Gyr and investigates the collisions.
The total number of objects needed to be integrated according to section 6.2 and section 6.3 is of the order of $10^4 - 10^7$, which is too much considering the computational time. Therefore the number of IMBHs is set to 500 and scaled up afterwards accordingly, as described below. The molecular cloud population is simulated in full number.

The IMBHs, having compared to the molecular cloud radii a negligible Bondi-Hoyle radius (see section 3.2), are treated as point objects. As long as an IMBH is inside any molecular cloud, defined as $(\Delta r \,/\, R_{cloud}) < 1$ with Δr the distance between cloud and IMBH and R_{cloud} defined as in (49), 6 % of the time spent inside is considered to be 'shining time' with the luminosity calculated according to (26); if the Eddington limit (33) is overstepped, the Eddington luminosity is used instead. The reduction towards 6 % is due to the accretion oscillations mentioned in section 2.3 found in hydrodynamical simulations done by Park & Ricotti (2011). After 10 Gyr, the shining time of all IMBHs is summed up with respect to the associated (binned) luminosity L_i. The binning of the luminosity L is defined as

$$L \in L_i \text{ if } i < log_{10}(L) \leqslant i + 1 \tag{81}$$

This total shining time is then divided by the integration time of 10 Gyr, resulting in the fraction of time spent in clouds producing the respective luminosity range. This quantity, called $\bar{S}'(L_i)$, can be interpreted as the average expected number of IMBHs emitting at any given time with $L \in L_i$. As an example, a value of $\bar{S}'(L_i) = 2$ indicates, that in total within the 10 Gyr integration time so many IMBHs have been accreting in the luminosity range L_i, that, if they would shine all after each other, 20 Gyr of shining time has been produced. This can be understood as the average, that permanently 2 IMBHs are accreting with $L \in L_i$ within the 10 Gyr integration time.
As a last step, the resulting $\bar{S}'(L_i)$ is then multiplied by the factor $\bar{S}(L_i) = \frac{N_{(1,2)(A,B)}}{500} \cdot \bar{S}'(L_i)$, with $N_{(1,2)(A,B)}$ corresponding to the model in (79), in order to take the reduced number of IMBHs into account. This assumes that the masses and orbits covered by the 500 IMBHs are representative. A plot of the resulting $\bar{S}(L_i)$ versus the luminosity bins L_i for the four different setups is shown in figure 17, top. Blue straight lines correspond to setup (A,1), blue dashed to (A,2), red straight to (B,1) and red dashed to (B,2). The error bars follow $\sqrt{N_i}$ with N_i the number of collisions resulting in the luminosity bin L_i, and are only shown for setups (A,1) and (B,1) for clarity. 18.6% of all collisions result in luminosities higher than the Eddingtion limit and needed to be capped, causing the peak for $10^{40} < L < 10^{41}$. This encourages the consideration of super-Eddington emissions.

Note here, that the difference between setups (X,1) and (X,2) does only affect the total number of cluster as represented by the proportional factor γ in equation (78), but not their mass distribution. This follows directly from equation (80), which is independent of γ. Consequently, the blue dashed lines are always 5% above the blue straight lines, the red dashed lines always 5% above the red straight lines. Similarly, an assumption that 5% of the stars are not born in cluster results in additional 5% difference compared to the results shown. This gives a sense about the degree of sensitivity of the results on the initial assumptions.
In order to investigate the effect of the different mass distributions assumed in the cases A and B, the fraction of the unmodified expected number of IMBHs, $s'(L_i) = \frac{\bar{S}'_A(L_i)}{\bar{S}'_B(L_i)}$ can be calculated. This assumes both cases, A and B, only consist of 500 IMBHs and allows direct comparsion between the resulting shining times since the number of objects is identical and only the mass distribution is different. Unsurprisingly, for low luminosities ($10^{34}\frac{erg}{s} < L < 10^{35}\frac{erg}{s}$) this value is low with $s'(L_{34}) = 0.8$, meaning only 80% of the shining time in this luminosity range of case B is achieved in case A. Since case B allows smaller cluster masses, and due to the dependency of $N \propto \frac{1}{M_{cls}}$ in equation (80), lighter cluster creating lighter IMBHs take a higher fraction within the whole population for case B than for case A. This then results in more low luminosity events. Consequently, the trend reverses for higher luminosities: in case A more massive IMBHs are present than in case B, causing $s'(L_{41}) = 1.4$. In the middle, $34 < i < 41$ the ratio is about constant 1, meaning the statistic is too noisy in this region to follow a linear increase from 0.8 to 1.4.
Figure 17, bottom, visualizes the contribution of each actually simulated IMBH (500 in total) towards $\bar{S}'(L_i)$. The x-axis refers to the (unbinned) luminosity, the y-axis to the mass of the IMBH causing this luminosity in a cloud collision. Each blue data point represents one cloud collision (3329 in total) with the IMBH/cluster mass distributed according to case A (Note: setup (A,1) and setup (A,2) follow the same mass distribution, therefore produce here an identical plot), the red data points represent the same collisions but the IMBH/cluster mass distribution follows case B. The green line corresponds to the Eddington limit. For clarification: The resulting shining time caused by each of the collisions summed up and scaled up with the factor $\frac{N_{(1,2)(A,B)}}{500}$ produces figure 17, top. Figure 17 bottom reveals, that in both mass distributions no IMBH is assigned a mass higher than about $3 \cdot 10^4 M_\odot$, although the upper limit in both distributions is $10^{7.5} M_\odot$, hinting towards a low impact of high mass cluster/IMBHs due to the mentioned $N \propto \frac{1}{M_{cls}}$ relation. In general, the constructed mass distribution of IMBHs, either following case A or B, results in reasonable IMBH masses between $100 M_\odot$ and $3 \cdot 10^4 M_\odot$ with a bias towards lower masses. This bias is higher for case B, causing only two IMBHs with $M_{BH} > 5 \cdot 10^3 M_\odot$ while case A causes eight; consequently, case B produces more low mass IMBHs.
This enables the conclusions, that different assumptions for the mass of the in the cluster growing IMBHs (73) does not significantly change the result qualitatively, only quantitatively due to different N (equation (79)); this effect of different N dominates the compared to this small difference of up to 40 % due to the shifted mass distribution.
This can be compared to an assumed constant IMBH mass distribution with $M_{BH} = 100 M_\odot$ for all IMBHs. The luminosity distribution resulting from this example is plotted in figure 18, assuming the same number of IMBHs as used in figure 17 and defined in (79). The Eddington limit restricts the luminosity to be lower than $1.26 \cdot 10^{40}\frac{erg}{s}$. The peak luminosity shifts into the bin L_{38}.

The most influential and not yet addressed parameter in this investigation is the fraction f of massive enough star cluster which indeed produce an IMBH; so far this value is set to $f = 100\%$. As evidently following from figure 17, this results in the prediction of several (case A) to several tens (case B) ULX sources ($L > 10^{39}\frac{erg}{s}$) permanently visible today. Since this is not the case (section 2.7) but X-Ray sources of lower luminosity are indeed observable, f needs to be adapted accordingly. This is addressed along with a quantitative investigation of figure 17, top, and figure 18 in the next section.

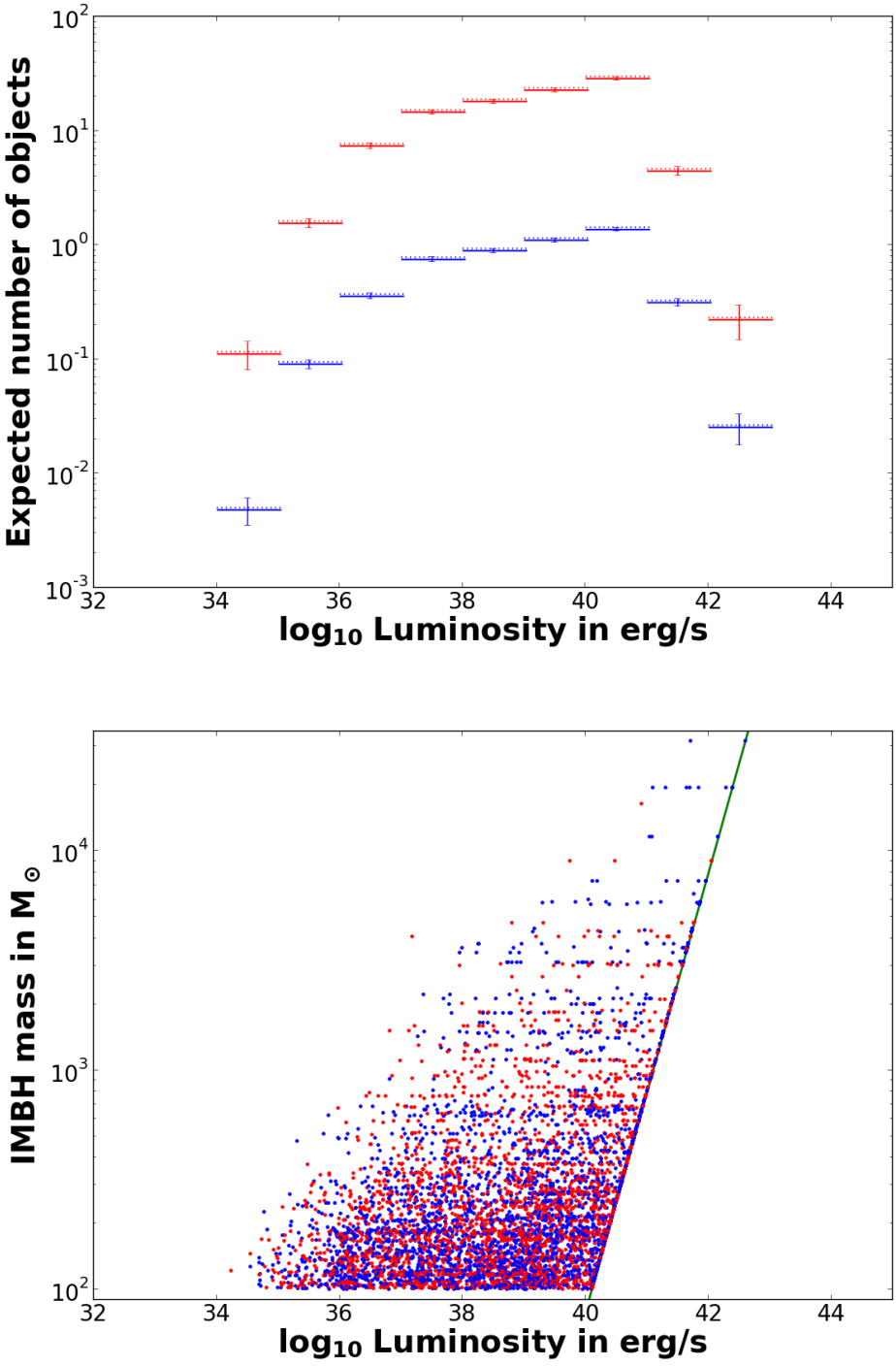

Figure 17: *Top: $\bar{S}(L_i)$ versus the binned luminosity L_i (see text). Straight blue: setup (A,1), dashed blue: setup (A,2), straight red: setup (B,1), dashed red: setup (B,2). (setups defined in (79)). Bottom: IMBH mass in each cloud collision versus the resulting luminosity; see text for details. Blue: IMBH mass distribution following case A, red: distribution following case B.*

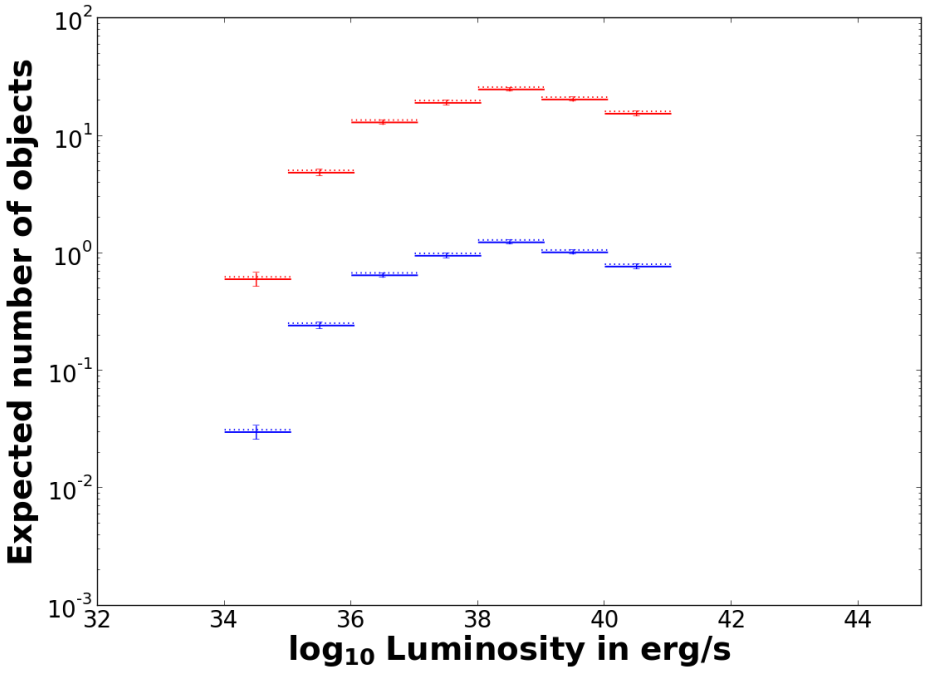

Figure 18: $\bar{S}(L_i)$ *versus the binned luminosity* L_i *assuming all IMBHs have a mass* $M_{BH} = 100M_{\odot}$. *The number of IMBHs follows the four different setups as in figure 17. Straight blue: setup (A,1), dashed blue: setup (A,2), straight red: setup (B,1), dashed red: setup (B,2))*

6.5 Comparison with observations

This section is dedicated to the investigation whether or not the results from figure 17 are possible to be scaled in a way, that the predictions match with the current observations. If so, a fraction of the observed X-Ray binary sources which are not confirmed binaries might be identified as IMBHs accreting in molecular clouds. The scale factor investigated for this purpose is the even in terms of magnitudes unknown factor f, the ratio between the cluster capable of creating IMBHs and the cluster indeed creating IMBHs. For simplicity, f is assumed to be independent from the cluster mass. This implies that f is directly proportional to $\bar{S}(L_i)$.

Following the optimistic case B with 839934 (879930) IMBHs present in the Milky Way today, figure 17 predicts the permanent visibility of in total 56.3 (59.0) X-Ray objects with luminosities $L \geqslant 39$ (ULX luminosities, see section 2.7). Case A predicts 2.84 (3.14) objects. Since no ULX are observable in the Milky Way today, this gives a first estimation for f: $f_A < 0.35$ and $f_B < 0.018$ would result in less than 1 predicted ULXs.
Another constrain can be provided by comparing the number of observed X-Ray sources in the galaxy with the predicted. For that purpose, all HMXB and LMXB found in literature (see section 2.4) which have no orbital period given are considered to be not confirmed X-Ray binaries and therefore possible candidates for in molecular clouds accreting IMBHs. Additionally, only X-Ray sources in the galactic disc are considered in order to enable comparability with the thin disc simulation. Since for most of the HMXB and LMXB sources the distance from the sun is not known, this constrain is applied in the way, that only sources with galactic latitudes smaller than 5° and bigger than −5° are considered. This translates into a reasonable disc height of 400 pc at a distance from the sun of $5kpc$; a lower angle might cut out sources close to the sun.
Figure 19 visualizes the selected X-Ray sources in an Aitoff projection of the galaxy. The Aitoff pro-

jection maps the galactic longitude, l, and latitude, b, onto a 2:1 ellipse with the galactic center in the middle. The advantage of an Aitoff projection is, that distance and orientation of each point towards the galactic center are compared to other points proportionally correct. An Aitoff projection is defined as

$$\begin{aligned} x_{Ait} &= \frac{2\alpha \cos(b) \sin(\frac{l}{2})}{\sin(\alpha)} \\ y_{Ait} &= \frac{\alpha \sin(b)}{\sin(\alpha)} \end{aligned} \tag{82}$$

with

$$\alpha = \arccos\left(\cos(b)\ \cos\left(\frac{l}{2}\right)\right) \tag{83}$$

and x_{Ait}, y_{Ait} the transformed coordinates as seen in figure 19.

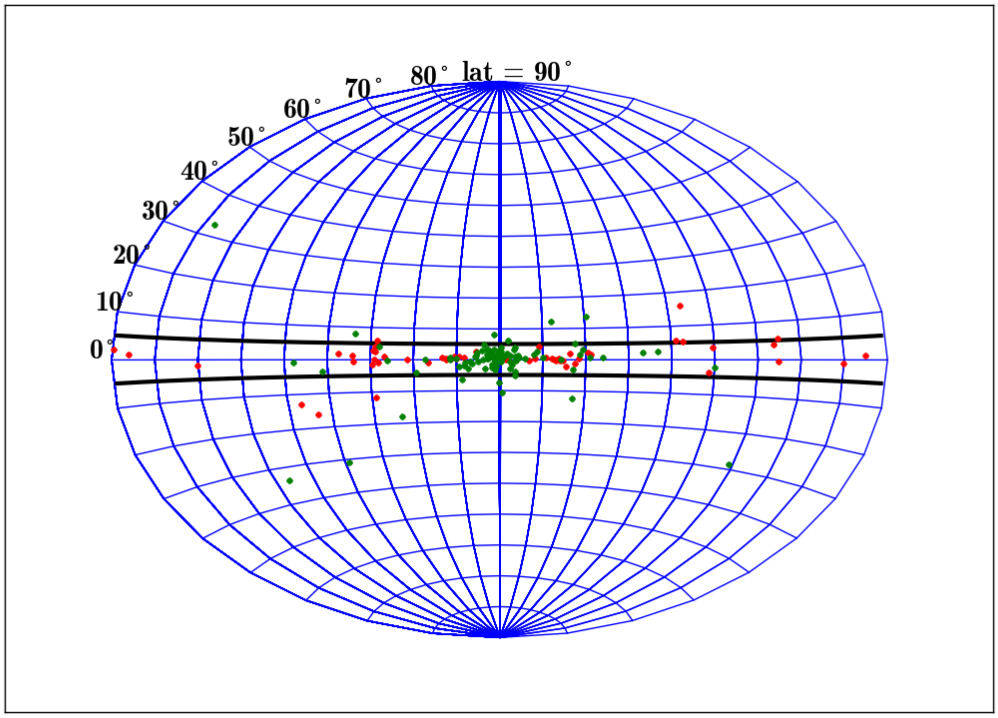

Figure 19: *Aitoff projection of the galaxy with the galactic center in the middle. Galactic longitude increases from left* $(-90°)$ *to right* $(+90°)$*, galactic latitude as shown. Plotted are the HMXBs (red) and LMXB (green) with no known orbital period. These objects are here considered to be non-binary X-Ray sources. The black lines include all sources with* $-5° <$ *latitude* $< 5°$.

The total number of HMXBs and LMXBs with unknown orbital period is 177, from that 155 are within $-5° < b < 5°$. The luminosity of the X-Ray objects with known distance reaches up to luminosities of several $10^{38} \frac{erg}{s}$. The thin disc simulation carried out in this section results for non-ULX objects ($L < 10^{39} \frac{erg}{s}$) into expected 2.1 (2.2) objects for setups (A,1) ((A,2)) and 41.9 (43.9) for case (B,1)

((B,2)) as shown in figure 17.
This result does not constrain f in any way for case A; even if the massive cluster produce IMBH with 100% efficiency, only a fraction of 1% of the observed possibly non-binary X-Ray sources are expected to be in molecular cloud accreting IMBHs. However, if so, then also about 3 objects with $L > 10^{39} \frac{erg}{s}$ are expected, of which none is observed. Therefore, the most optimistic estimation for f can only be $f_{A,1} < \frac{1}{2.84} = 0.35$ ($f_{A,2} < 0.32$), resulting in one predicted ULX which can be considered in agreement with the observations. In this case, also about 1 object with $L < 10^{39} \frac{erg}{s}$ is expected, which is of course also consistent with observations.
For case B, the expected number of non-ULX objects are equal to about 25% of the observed non-binary X-Ray sources for $f_B = 1$. However, this implies as mentioned in turn 56.3 (59.0) ULXs. Again here the not existing ULX in the Milky Way constrain f_B, $f_{B,1} < 0.018$ ($f_{B,2} < 0.017$) for only one expected ULX at any given time. This then results into 0.75 (0.75) expected objects with $L < 10^{39} \frac{erg}{s}$. If case A and B are regarded as extreme assumptions with a realistic relation between $M_{cluster}$ and M_{IMBH} somewhere in the middle, then $0.017 < f < 0.35$.
Even if it is assumed that each cluster produces an identical IMBH with the mass of 100 $M_\odot$ as seen in figure 18, ULX luminosities, meaning here accretion close to the Eddington limit, confines f most. Here, $f_{A,1} < 0.56, f_{A,2} < 0.53$ resulting in one expected ULX and 1.7 (1.8) expected objects with $L < 10^{39} \frac{erg}{s}$. For case B, $f_{B,1} < 0.028, f_{B,2} < 0.027$ cause one ULX and 1.74 (1.74) low luminosity X-Ray sources. Therefore, the restriction applied by the not observed ULXs in the Milky Way is an inherit problem for IMBHs in general and can not be overcome by using IMBHs with a low mass.

The results of section 6 can therefore be summarized as:

- Different assumptions about the fraction of cluster mass ending up in IMBHs changes most significantly the total number of expected objects, the shifted mass distribution has only a minor impact.
- The IMBH creation efficiency f in cluster is constrained by the lack of ULXs in the Milky Way for all assumed IMBH mass distributions: $f_A < 0.35$, $f_B < 0.017$.
- If f is constrained via the number of ULXs, then less than 1 X-Ray sources in the Milky Way with $L < 10^{39} \frac{erg}{s}$ is expected to be caused by in molecular clouds accreting IMBHs.

7 Cluster destruction

7.1 Overview

In this section, the disruptive effect of multiple molecular cloud encounters on star cluster is investigated. Gieles et al. (2006) derived a single expression for the energy gain in star cluster depending on the impact conditions. This expression is applied on the globular cluster (section 4) and the disc-like cluster (section 6) simulated for 10 Gyr using the 3D model presented in section 6.2. Other disruptive effects, such as two body relaxation, mass loss due to stellar evolution or gas expulsion are not considered (Gieles, 2010).

7.2 Cluster energy gain in molecular cloud encounter

Gieles et al. (2006) performed N-body simulations of star cluster while encountering a molecular cloud. They used the results to motivate and verify the adoption of an analytical closed formular for the total energy gain ΔE in the cluster due to the encounter.
Their resulting formular is an extrapolation from previous works in this context, namely from Spitzer (1958) and Binney & Tremaine (1987) and is given as

$$\Delta E = \frac{4.4\ R_{cls}^2}{\left(p^2 + \sqrt{R_{cls}\ R_{cloud}^3}\right)^2} \left(\frac{GM_{cloud}}{v_{rel}}\right)^2 M_{cls} \tag{84}$$

with M_{cls} the mass and R_{cls} the radius of the cluster, M_{cloud} the mass and R_{cloud} the radius of the molecular cloud, and p the closest distance between cloud and cluster upon collision.
The initial energy of the cluster E_0 can be derived using the results from section 4.2. Assuming a $\frac{1}{r}$ density profile (40) for the cluster, virial equilibrium between kinetic energy T (44) and gravitational potential U (47) results in

$$2T = -U \tag{85}$$

$$\rightarrow M_{cls}\sigma^2 = \frac{4}{9}\frac{GM_{cls}^2}{R_{cls}} \tag{86}$$

with σ the velocity dispersion of the cluster. The total energy E_0 is then given as

$$E_0 = |T + U| = |\frac{1}{2}M_{cls}\sigma^2 - \frac{4}{9}\frac{GM_{cls}^2}{R_{cls}}| = \frac{2}{9}\frac{GM_{cls}^2}{R_{cls}} \tag{87}$$

Note that Gieles et al. (2006) used a plummer model (Plummer, 1911) for the density distribution and derives $E_0 \approx 0.19\ \frac{GM_{cls}^2}{R_{cls}}$.
Fit to observations done by Larsen (2004) revealed a mass-radius relationship for star cluster of

$$R_l = 1.12 \left(\frac{M_{cls}}{M_\odot}\right)^{0.1} \quad pc \tag{88}$$

with R_l the half-light radius of the cluster. Given the different observed density profiles, Portegies Zwart et al. (2010) suggests $R_{cls} = 1.625 R_l$ as a standard relation widely used.
Although this mass-radius relation has been derived from young stellar clusters in different spiral galaxies, it is used in this project as an approximation for both the globular cluster radii and the radii of the cluster in the disc.
The fractional energy gain of a cluster due to an encounter with a molecular cloud is defined as $E_f = \frac{\Delta E}{E_0}$. The fractional energy gain translates into increased motions of stars inside the cluster, leading to stars escaping the gravitational potential. This in turn decreases the total cluster mass; most energy is in fact lost in stars escaping with high velocities far above the velocity dispersion. The N-body simulations done by Gieles et al. (2006) reveal, that a fractional energy gain of about 10 corresponds to a mass loss equal to the total cluster mass. This represents the upper limit at which the cluster can be considered destroyed. In the following sections the cumulative effect of energy gains on cluster due to several collisions is investigated. In order to give an upper limit for the time until the cluster is destroyed, M_{cls} is considered to be constant, ignoring the effect of decreasing mass between encounters.

7.3 Results

7.3.1 Globular cluster

The globular cluster for which position and proper motions are known (63 in total) together with the 5227 molecular clouds of the 3D model have been integrated for 10 Gyr. Each time a cloud is hit, defined as $\Delta r < R_{cloud}$ with Δr the distance from the cluster midpoint to the cloud midpoint, the fractional energy gain $\frac{\Delta E}{E_0}$ as defined in (84) and (87) is calculated. The sum of all fractional energy gains due to cloud encounters within the 10 Gyr is plotted for each globular cluster in figure 20, top. The clusters are sorted on the x-axis according to their mean distance from the galactic center $R = \sqrt{x^2 + y^2}$ while the hits occur. This sorting is visualized in the bottom plot, in which the same ordering of the globular cluster is used; the y-axis shows the corresponding mean distance from the galactic center. A direct plot of the fractional energy gain versus the mean distance from the galactic center is not desirable due to the high number of data points within the molecular ring ($4 - 6kpc$). Note that 19 globular cluster have fractional energy gains of $\frac{\Delta E}{E_0} \leqslant 10^{-5}$ and are not shown for better clarity in the high energy gain cases. A energy gain of zero corresponds to no hit. In this case, the mean distance from the galactic center of the cluster orbit is used for the sorting process.
As mentioned and as the sorting of the cluster reveals, most cluster with high energy gains collide with clouds in the molecular ring. Outside the ring, beyond $6kpc$, the fractional energy gain systematically decreases, implying less collisions due to the lack of clouds. Mean (orbital) distances below $3kpc$ result in a step jump due to the absence of clouds (compare figure 5). The two globular cluster with exceptional high energy gains are NGC 6838 ($\frac{\Delta E}{E_0} = 9.7$) and NGC 5927 ($\frac{\Delta E}{E_0} = 0.7$). For NGC 6838, figure 8 visualizes the disc-like nature of the orbit exactly within the molecular ring, making collisions likely and the high energy gain reasonable. The fact, that the cluster is observable and has not been destroyed within its lifetime of $14 - 16Gyr$ (Hodder et al., 1992) as the fractional energy gain of 9.7 within 10 Gyr suggest, leads to the conclusion that the cluster has been more massive in the past. Indeed, the todays observed mass for NGC 6838 is 36700 $M_\odot$ (Harris, 1996) while the mean mass of all here investigated cluster is with 450851 $M_\odot$ one magnitude higher. The energy gain of the other globular cluster is compared to this example insignificant; a fractional energy gain of 0.1 corresponds only to a mass loss of about 1%. To conclude:

- With the exception of NGC 6838, globular cluster are not expected to suffer significant mass losses or even destruction due to molecular cloud encounters within 10 Gyr.

7.3.2 Thin disc cluster

The main difference between globular cluster and thin disc cluster in terms of molecular cloud collision is the frequency with which they collide with clouds and the relative velocity by doing so. The mean number of cloud collisions averaged over the globular cluster population within 10 Gyr is 1.3 collisions per cluster (with many cluster having no collisions), the mean number averaged over the thin disc cluster population is 6.7 collisions per cluster. Additionally, as shown before, the relative velocity v_{rel} is expected to be lower. According to equation (84), the fractional energy gain with lower v_{rel} is higher. Combining the higher collision probability and lower v_{rel}, thin disc cluster are expected to be destroyed on far shorter timescales than the globular cluster. This section derives a lower limit of survived star cluster with the probability to host an IMBH until today by assuming a destruction if $\frac{\Delta E}{E_0} > 1$.

Case A and case B as defined in section 6.3 produce different cluster destruction probabilities, because case A assumes only cluster with $M_{cls} > 50000 M_\odot$ are capable to host IMBHs, while in case B cluster are assigned with masses $M_{cls} > 2500 M_\odot$. Since according to equation (84) more massive cluster are expected to survive longer, differences between both cases are to be expected. Note that the mass distribution of the cluster is independent of whether scenario 1 or 2 is used since these scenarios only determine the total number of cluster, as expressed in the scale factor γ in equation (78). The mass distribution, defined in (80), is independent of γ.
Figure 21, top, presents the total fractional energy gain for 500 simulated thin disc cluster populated in the same way as in section 6 within 10 Gyr. The cluster mass is distributed following case A (blue), or case B (red), both distributions are applied towards the same simulation, revealing directly the impact

of different cluster masses. The total fractional energy gain of a cluster is the sum of all individual fractional energy gains calculated upon collision according to (84) and (87), with a collision defined as $\Delta r < R_{cloud}$ with Δr the distance from the cluster midpoint to the cloud midpoint. The energy gains of the clusters are plotted against a column of numbers in the order of increasing mean distances from the galactic center; figure 21 bottom translates the column of numbers into the mean distances.
Analog to the globular cluster case, mean distances in the molecular ring result reliable into higher energy gains. However, also outside the ring destruction due to single close encounters are possible. If $Q(t)$ is defined as the fraction of cluster destroyed after the time t in the simulation has passed, then $Q(10\ Gyr) = 0.68$ for case A, meaning 68 % of all cluster are destroyed within 10 Gyr. (Case B: $Q(10\ Gyr) = 0.74$).
In order to find out the fraction of cluster which possibly created an IMBH within their lifetime and are still alive today, the different points in time at which the cluster are formed need to be taken into account. If s is a random number in the interval $s \in [0, 1]$ and Q^{-1} is the inverse function of Q, then

$$l = Q^{-1}(s) \tag{89}$$

can be interpreted as a lifetime l of an individual cluster. The lifetime is therefore chosen in the following way: if a whole cluster population is associated with l with different random numbers s for each cluster, the cluster destruction fraction depending on time follows $Q(t)$. As a next step, the total lifetime of the Milky Way is discretized in time steps Δt with $n \cdot \Delta t = 10\ Gyr$. Assuming now at each time step $i \cdot \Delta t$ are N cluster born and each cluster is associated with an individual lifetime $l(s)$, and all cluster overstepping their lifetime are destroyed, then the total number of 'alive' cluster for each time step $N_a(t = i \cdot \Delta t)$ with $i = (1, ..., n)$ can be determined. A cluster is considered alive if it has already been created and its lifetime is not yet overstepped. The fraction

$$\frac{N_a(i\Delta t)}{N \cdot n} \tag{90}$$

then represents for i = n the fraction of cluster which are possibly able to create an IMBHs within their lifetime and are still alive today. Figure 22 shows a plot of (90) for $\Delta t = 20\ Myr$ and $N = 5000$. As a result, in case A (blue), 51% of all cluster which can possibly contain an IMBH are after $10Gyr$ (= today) not destroyed due to molecular cloud collisions. The different mass distribution in case B (red), allowing lighter cluster to create IMBHs, results in only 46% still intact cluster, mirroring the implication of equation (84) and (87), that lighter cluster are destroyed faster. In conclusion,

- Star cluster within the thin disc are likely to be destroyed due to molecular cloud collisions: For case A, after t = 10 Gyr, 68% off all cluster which have been present since t = 0 have been destroyed (74% for case B)
- Taking into account star cluster are born successively during the lifetime of the Milky Way, only 49% (case A) off all cluster born until t = 10 Gyr have been destroyed (54% for case B), implying that about half of all IMBHs which have been created in star cluster have already lost their host.

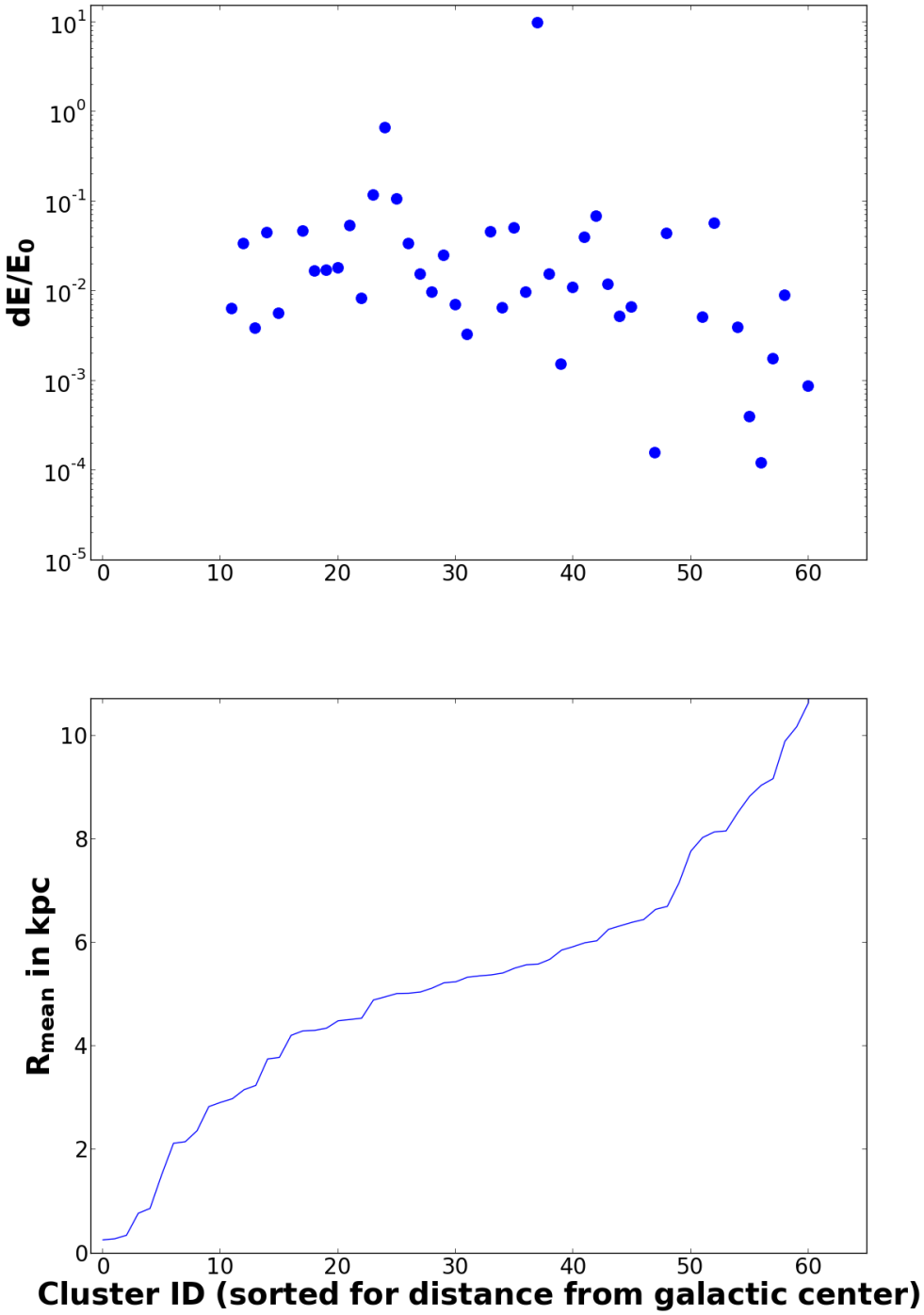

Figure 20: *Top: Fractional energy gain* $\frac{\Delta E}{E_0}$ *due to molecular cloud collisions of globular cluster versus a column of increasing numbers. The globular cluster are associated with the numbers in the order of increasing mean distance from the galactic center* R_{mean} *while the collisions occur. Bottom: The same column of numbers plotted versus* R_{mean} *of the corresponding globular cluster.*

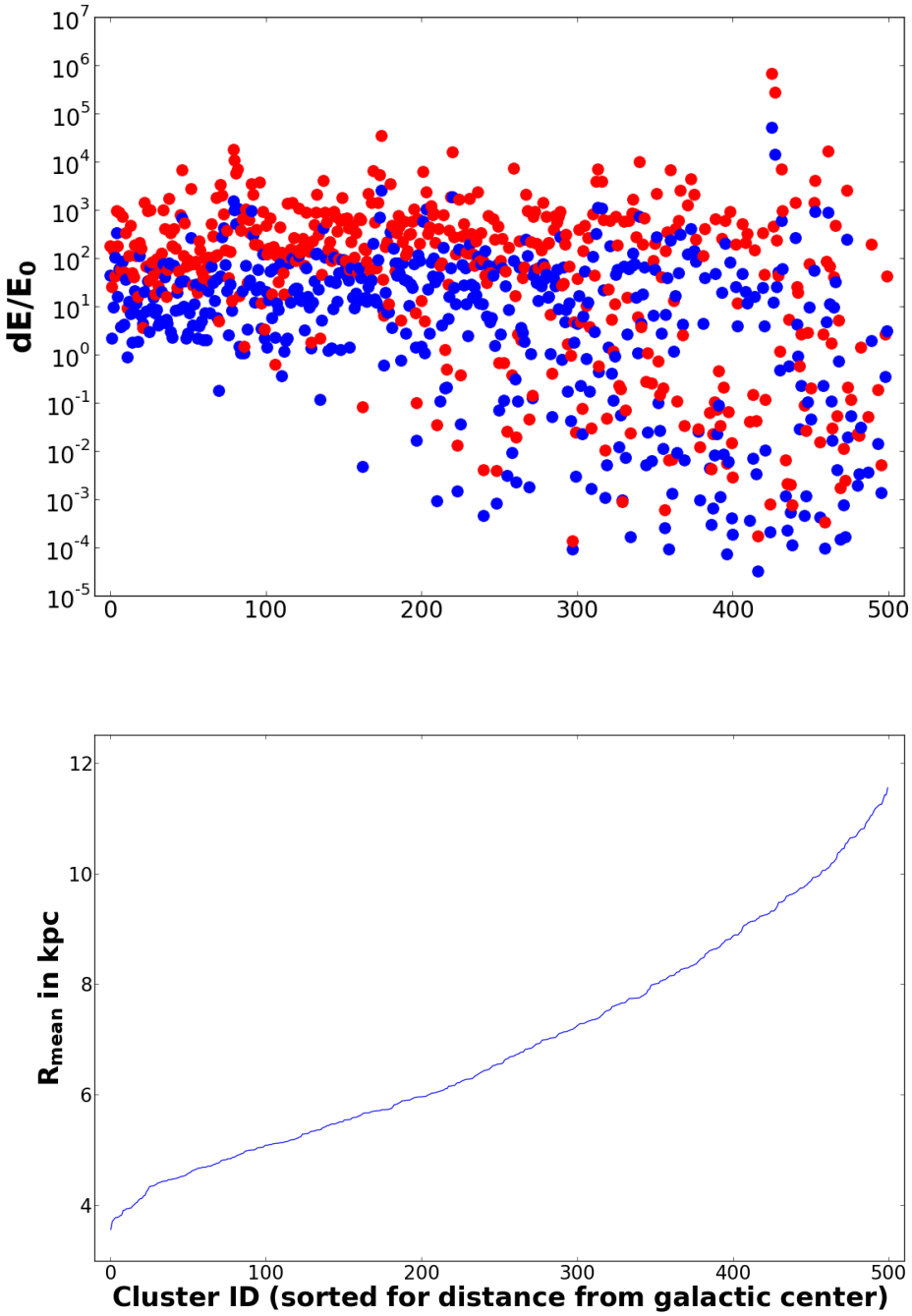

Figure 21: *Top: Fractional energy gain* $\frac{\Delta E}{E_0}$ *due to molecular cloud collisions of 500 thin disc cluster versus a column of increasing numbers. The cluster are associated with the numbers in the order of increasing mean distance from the galactic center* R_{mean} *while the collisions occur. Blue: the cluster mass distribution follows case A. Red: case B. Bottom: The same column of numbers plotted versus* R_{mean} *of the corresponding cluster. Note that this curve is identical for case A and B since different cluster masses do not affect the position of collisions with molecular clouds.*

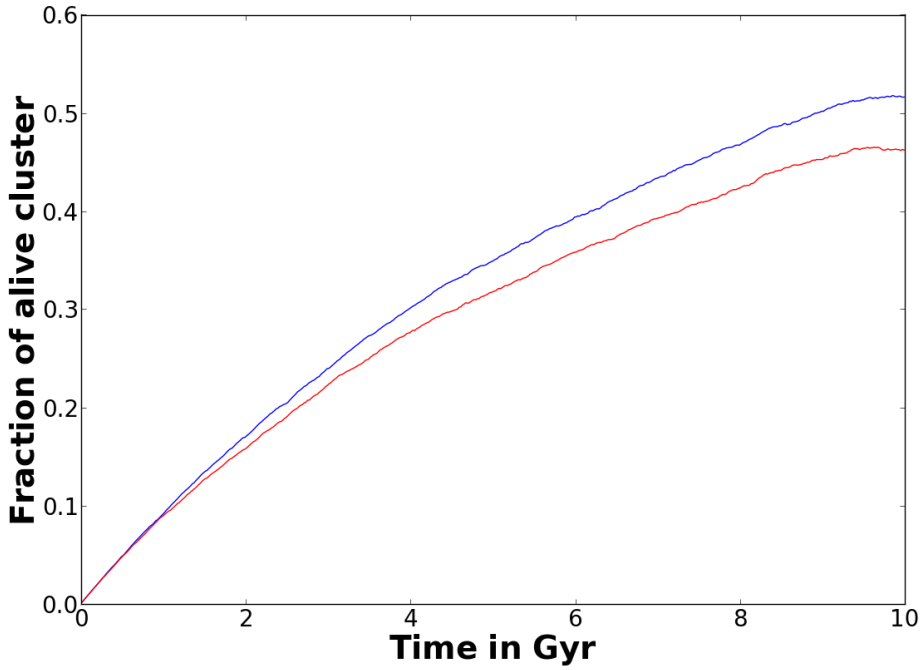

Figure 22: *Fraction of alive (= not destroyed and already created) cluster over the total number of star cluster born in the whole lifetime of the Milky Way. Blue: cluster mass distribution and therefore $Q(t)$ following case A. Red: case B.*

8 Summary

This project investigates the possible impact of different assumed IMBHs populations in the Milky Way. The idea followed is, that IMBHs create detectable X-Ray luminosities while passing through molecular clouds in the galactic disc.
The modeling of the resulting luminosity in an accretion process within a molecular cloud revealed, that, assuming Bondi-Hoyle accretion as an upper limit, the luminosity critically depends on the relative velocity $L \propto v_{rel}^{-3}$ between IMBH and cloud and is almost insensitive to the cloud mass, $L \propto M_{cloud}^{-0.43}$. For luminosities in the ULX regime, $v_{rel} < 100 \frac{km}{s}$ are required.
The orbits of three different assumed IMBH populations have been numerically integrated for 10 Gyr. For each collision with a molecular cloud, v_{rel} has been measured and translated into a luminosity.
As a first step, globular cluster orbits have been used as an analogy for the unknown IMBH orbits representing objects located mostly outside the galactic disc. Therefore, the orbit and resulting cloud collisions of each globular cluster for which position and proper motions are known (63 in total) have been investigated. The probability to hit a cloud while crossing the galactic disc is highest within the molecular ring located at a distance from the galactic center of about 4-6 kpc; the high concentration of clouds in this ring results in a collision probability of about 3%. With the exception of NGC 6838, no globular cluster orbit achieves v_{rel} below $80 km/s$, resulting, if an IMBH mass of $M_{BH} = 10^4$ is assumed, in luminosities below $10^{39} \frac{erg}{s}$. Although NGC 6838 can potentially create an ULX, the fraction of time shining with such a luminosity ('shining time') is below 10^{-4} years per year, making single IMBHs, such as IMBHs residing in fact within globular cluster, difficult to detect via this mechanism. However, if a sufficient high number of IMBHs on globular cluster orbits are assumed, then a cloud collision with any of them becomes likely enough so that at any given time one X-Ray object can be expected to be observed. Quantitatively, if the shining time is averaged over the whole globular cluster population (resulting in $3 \cdot 10^{-6}$ years per year), then $3.3 \cdot 10^5$ IMBHs are required to produce on average one X-Ray object at any given time.
An inherit flaw of the globular cluster analogy is the low number of available orbits to investigate. The next step in this project increases this number by creating an artificial population based on the globular cluster orbits but with random inclinations α towards the galactic disc, resulting in total in 1260 different orbits. As intended, this random population is a meaningful extension of the globular cluster population and creates similar results in terms of v_{rel} but with less statistical noise due to too low numbers. It is confirmed that v_{rel} below $100 \frac{km}{s}$ for those halo-like orbits is only rarely achieved (in 1.3% of all collisions). ULX luminosities are therefore rare and only reached during 9 different collisions. The mean relative velocity averaged over all collisions is $356.3 \frac{km}{s}$. The mean shining time compared to the globular cluster value corrects down to $1.9 \cdot 10^{-6}$; the number of IMBHs required to orbit in the same way as the random population in order to create on average one X-Ray object at any given time changes therefore to $5.3 \cdot 10^5$. Given Rashkov & Madau (2014) theorized 70 to 2000 IMBHs should be present today in the Milky Way halo assuming massive black hole seeds were common during galaxy formation (which could explain the fast growth of supermassive black holes), then this work concludes, that only in a small fraction of time, namely $1.3 \cdot 10^{-4}$ up to $3.8 \cdot 10^{-3}$ years per year, one of those halo-like IMBHs should be observable as X-Ray object in the galactic disc due to accretion within molecular clouds. This means the search for halo-like IMBHs via this mechanism would be nearly impossible.
If $\bar{v}_{rel}$ is defined as the mean relative velocity averaged over all collisions of one particular IMBH, then the random population additionally proves a direct relation between $\bar{v}_{rel}$, the inclination angle α and the orbit eccentricity e. Given this, the orbits with the highest expected relative velocities have been identified as disc-like orbits defined as orbits with $\alpha < 20°$ and $e < 0.4$.
This leads to the last investigated assumed IMBH population, the disc-like population. It is assumed that each star cluster with sufficient high mass can create within its center an IMBH with the probability f. Given this and tracing back the cluster formation process towards the beginning of the Milky Way, then, with f = 1 (meaning 100 %), between 41934 (case A) and 879930 (case B) IMBHs can be expected to be present today in the Milky Way, depending on the lowest cluster mass which still enables the cluster to create an IMBH. Simulating this population reveals, that about 3 (case B: almost 60) ULX should be visible at any time in the Milky Way. Given that no ULX are observed today, this in turn constrains f towards $f_A < 0.35$ and $f_B < 0.018$. Freitag et al. (2006) performed N-body simulations

investigating the core collapse into massive objects within cluster and concluded, that presumably more than 20% of all globular cluster indeed created IMBHs in an early stage ($\approx$ few Myr) of their formation. Using their assumptions (case A), this work concludes, that for (open) cluster within the disc, less than 35% of all cluster can create IMBHs. This work therefore provides an upper limit on the lower limit given in literature by investigating the observational consequences of too high f.
Applying this constrain, less than 1 non-X-Ray source ($L < 10^{39} \frac{erg}{s}$) is expected to be visible at any given time. Therefore, only less than 0.6 % of all today observed X-Ray sources in the Milky Way disc are expected to be caused by in molecular clouds accreting IMBHs. This proves, that a detection of disc-like IMBHs is as difficult as the detection of halo-like IMBHs using the effect of X-Ray creation within molecular clouds. This also implies, that no more than 14677 (case B: 15839) IMBHs are expected to be present within the galactic disc, otherwise one ULX would be expected to be observable at any given time.
About 49 % (case B: 54 %) of the in the disc present IMBHs which have been formed during the lifetime of the Milky Way within star cluster cores have already lost their host cluster due to perturbation during molecular cloud encounters. In a similar way, the globular cluster NGC 6838 is expected to be destroyed within 10 Gyr on its present orbit. Since the cluster with an age of $14 - 16 Gyr$ is evidently observed today, it had to be more massive upon creation than it is measured today. With the exception of NGC 5927, all other investigated globular cluster are expected to suffer a mass loss of only up to 1% due to molecular cloud encounters.

9 References

Allen, C., Pichardo, B. S., & Moreno, E. 2008, in Revista Mexicana de Astronomia y Astrofisica Conference Series, Vol. 34, Revista Mexicana de Astronomia y Astrofisica Conference Series, 107–110

Allen, C., & Santillan, A. 1991, Rev. Mexicana Astron. Astrofis., 22, 255

Begelman, M. C. 2002, ApJ, 568, L97

Binney, J., & Tremaine, S. 1987, Galactic dynamics

Bondi, H., & Hoyle, F. 1944, MNRAS, 104, 273

Caballero-García, M. D., Belloni, T., & Zampieri, L. 2013, MNRAS, 436, 3262

Carlin, J. L., Majewski, S. R., Casetti-Dinescu, D. I., et al. 2012, ApJ, 744, 25

Casares, J., & Jonker, P. G. 2013, Space Sci. Rev., arXiv:1311.5118

Casetti-Dinescu, D. I., Girard, T. M., Herrera, D., et al. 2007, AJ, 134, 195

Casetti-Dinescu, D. I., Girard, T. M., Jílková, L., et al. 2013, AJ, 146, 33

Casetti-Dinescu, D. I., Girard, T. M., Korchagin, V. I., van Altena, W. F., & López, C. E. 2010, AJ, 140, 1282

Chaty, S. 2013, Advances in Space Research, 52, 2132

Chiappini, C., Minchev, I., & Martig, M. 2013, in European Physical Journal Web of Conferences, Vol. 43, European Physical Journal Web of Conferences, 2001

Clemens, D. P., Sanders, D. B., & Scoville, N. Z. 1988, ApJ, 327, 139

Cudworth, K. M., Hanson, R. B., Majewski, S. R., & Schweitzer, A. E. 1993, in Astronomical Society of the Pacific Conference Series, Vol. 48, The Globular Cluster-Galaxy Connection, ed. G. H. Smith & J. P. Brodie, 80

Dewangan, G. C., Mathur, S., Griffiths, R. E., & Rao, A. R. 2008, ApJ, 689, 762

Dinescu, D. I., Girard, T. M., & van Altena, W. F. 1999a, AJ, 117, 1792

Dinescu, D. I., Girard, T. M., van Altena, W. F., & López, C. E. 2003, AJ, 125, 1373

Dinescu, D. I., Girard, T. M., van Altena, W. F., Mendez, R. A., & Lopez, C. E. 1997, AJ, 114, 1014

Dinescu, D. I., van Altena, W. F., Girard, T. M., & López, C. E. 1999b, AJ, 117, 277

Dowell, J. D., Buckalew, B. A., & Tan, J. C. 2008, AJ, 135, 823

Edgar, R. 2004, New A Rev., 48, 843

Fabbiano, G. 2006, ARA&A, 44, 323

Feldmeier, A., Lützgendorf, N., Neumayer, N., et al. 2013, A&A, 554, A63

Freitag, M., Rasio, F. A., & Baumgardt, H. 2006, MNRAS, 368, 121

Ghez, A. M., Salim, S., Weinberg, N. N., et al. 2008, ApJ, 689, 1044

Gieles, M. 2010, in IAU Symposium, Vol. 266, IAU Symposium, ed. R. de Grijs & J. R. D. Lépine, 69–80

Gieles, M., Portegies Zwart, S. F., Baumgardt, H., et al. 2006, MNRAS, 371, 793

González-Galán, A., Vilardell, F., Negueruela, I., et al. 2013, in Revista Mexicana de Astronomia y Astrofisica Conference Series, Vol. 42, Revista Mexicana de Astronomia y Astrofisica Conference Series, 30–31

Goswami, S., Umbreit, S., Bierbaum, M., & Rasio, F. A. 2012, ApJ, 752, 43

Haiman, Z. 2013, in Astrophysics and Space Science Library, Vol. 396, Astrophysics and Space Science Library, ed. T. Wiklind, B. Mobasher, & V. Bromm, 293

Harris, W. E. 1996, AJ, 112, 1487

Heyer, M., Krawczyk, C., Duval, J., & Jackson, J. M. 2009, ApJ, 699, 1092

Hodder, P. J. C., Nemec, J. M., Richer, H. B., & Fahlman, G. G. 1992, AJ, 103, 460

Hou, L. G., Han, J. L., & Shi, W. B. 2009, A&A, 499, 473

Hoyle, F., & Lyttleton, R. A. 1939, Proceedings of the Cambridge Philosophical Society, 35, 405

Inoue, Y., Tanaka, Y. T., Madejski, G. M., & Domínguez, A. 2014, ApJ, 781, L35

Irrgang, A., Wilcox, B., Tucker, E., & Schiefelbein, L. 2013, A&A, 549, A137

King, A. R., Davies, M. B., Ward, M. J., Fabbiano, G., & Elvis, M. 2001, ApJ, 552, L109

Kocsis, B., & Loeb, A. 2013, Space Sci. Rev., arXiv:1310.0815

Krolik, J. H. 2004, ApJ, 615, 383

Kuranov, A. G., Popov, S. B., Postnov, K. A., Volonteri, M., & Perna, R. 2007, Astronomical and Astrophysical Transactions, 26, 87

Lada, C. J., & Lada, E. A. 2003, ARA&A, 41, 57

Larsen, S. S. 2004, A&A, 416, 537

Larson, R. B. 1981, MNRAS, 194, 809

Law, D. R., & Majewski, S. R. 2010, ApJ, 714, 229

Liu, Q. Z., van Paradijs, J., & van den Heuvel, E. P. J. 2006, A&A, 455, 1165

—. 2007, A&A, 469, 807

Lützgendorf, N., Kissler-Patig, M., Gebhardt, K., et al. 2013, Mem. Soc. Astron. Italiana, 84, 129

Maccarone, T. J. 2004, MNRAS, 351, 1049

Madau, P., Haardt, F., & Dotti, M. 2014, ArXiv e-prints, arXiv:1402.6995

Makishima, K. 2007, in IAU Symposium, Vol. 238, IAU Symposium, ed. V. Karas & G. Matt, 209–218

Makishima, K., Kubota, A., Mizuno, T., et al. 2000, ApJ, 535, 632

Mayer, L., Kazantzidis, S., Escala, A., & Callegari, S. 2010, Nature, 466, 1082

McClintock, J. 2004, in APS April Meeting Abstracts, D3004

Mezcua, M., Fabbiano, G., Gladstone, J. C., Farrell, S. A., & Soria, R. 2014, ArXiv e-prints, arXiv:1403.1071

Miller, J. M. 2006, in Astronomical Society of the Pacific Conference Series, Vol. 352, New Horizons in Astronomy: Frank N. Bash Symposium, ed. S. J. Kannappan, S. Redfield, J. E. Kessler-Silacci, M. Landriau, & N. Drory, 121

Miller, M. C., & Hamilton, D. P. 2002, MNRAS, 330, 232

Misiriotis, A., Xilouris, E. M., Papamastorakis, J., Boumis, P., & Goudis, C. D. 2006, A&A, 459, 113

Miyamoto, M., & Nagai, R. 1975, PASJ, 27, 533

Noyola, E., Gebhardt, K., & Bergmann, M. 2008, ApJ, 676, 1008

Nyland, K., Marvil, J., Wrobel, J. M., Young, L. M., & Zauderer, B. A. 2012, ApJ, 753, 103

Odenkirchen, M., Brosche, P., Geffert, M., & Tucholke, H.-J. 1997, New A, 2, 477

Özel, F., Psaltis, D., Narayan, R., & McClintock, J. E. 2010, ApJ, 725, 1918

Paczynski, B. 1990, ApJ, 348, 485

Park, K., & Ricotti, M. 2011, ApJ, 739, 2

Peterson, B. M. 2013, Space Sci. Rev.

Pichardo, B., Martos, M., & Moreno, E. 2004, ApJ, 609, 144

Pichardo, B., Martos, M., Moreno, E., & Espresate, J. 2003, ApJ, 582, 230

Pintore, F., Zampieri, L., Wolter, A., & Belloni, T. 2014, MNRAS, arXiv:1401.6815

Piskunov, A. E., Kharchenko, N. V., Schilbach, E., et al. 2008, A&A, 487, 557

Plotkin, R. M., Markoff, S., Kelly, B. C., Körding, E., & Anderson, S. F. 2012, MNRAS, 419, 267

Plummer, H. C. 1911, MNRAS, 71, 460

Portegies Zwart, S. 2010, New A Rev., 54, 173

Portegies Zwart, S. F., & McMillan, S. L. W. 2002, ApJ, 576, 899

Portegies Zwart, S. F., McMillan, S. L. W., & Gieles, M. 2010, ARA&A, 48, 431

Prestwich, A. H., Kilgard, R., Crowther, P. A., et al. 2007, ApJ, 669, L21

Rashkov, V., & Madau, P. 2014, ApJ, 780, 187

Rybicki, G. B., & Lightman, A. P. 1979, Radiative processes in astrophysics

Scoville, N. Z., & Sanders, D. B. 1987, in Astrophysics and Space Science Library, Vol. 134, Interstellar Processes, ed. D. J. Hollenbach & H. A. Thronson, Jr., 21–50

Shu, C., Luo, Z., Han, M.-a., et al. 2010, Advances in Space Research, 46, 500

Solomon, P. M., Rivolo, A. R., Barrett, J., & Yahil, A. 1987, ApJ, 319, 730

Solomon, P. M., & Sanders, D. B. 1980, in Giant Molecular Clouds in the Galaxy, ed. P. M. Solomon & M. G. Edmunds, 41–73

Spitzer, Jr., L. 1958, ApJ, 127, 17

Sun, M.-Y., Jin, Y.-L., Gu, W.-M., et al. 2013, ApJ, 776, 118

Tanaka, T., & Haiman, Z. 2009, ApJ, 696, 1798

Umbreit, S., & Rasio, F. A. 2013, ApJ, 768, 26

Valencia-S, M., Eckart, A., Zuther, J., et al. 2012, Journal of Physics Conference Series, 372, 012048

Venemans, B. P., Findlay, J. R., Sutherland, W. J., et al. 2013, ApJ, 779, 24

Volonteri, M. 2010, A&A Rev., 18, 279

Volonteri, M., Madau, P., & Metcalf, R. B. 2003, in Bulletin of the American Astronomical Society, Vol. 36, American Astronomical Society Meeting Abstracts, 582

Webb, N. A., Barret, D., Braito, V., et al. 2012, in SF2A-2012: Proceedings of the Annual meeting of the French Society of Astronomy and Astrophysics, ed. S. Boissier, P. de Laverny, N. Nardetto, R. Samadi, D. Valls-Gabaud, & H. Wozniak, 631–636

Whitmore, B. C. 2009, Ap&SS, 324, 163

Zhang, S.-N. 2012, in COSPAR Meeting, Vol. 39, 39th COSPAR Scientific Assembly, 2261